

Origin of a late Neoproterozoic (605 ± 13 Ma) intrusive carbonate–albitite complex in Southern Sinai, Egypt

Mokhles Kamal Azer · Robert J. Stern ·
Jun-Ichi Kimura

Received: 7 February 2008 / Accepted: 26 October 2008 / Published online: 2 December 2008
© Springer-Verlag 2008

Abstract New geochemical, isotopic, and geochronological data and interpretations are presented for late Neoproterozoic intrusive carbonates and related rocks of southern Sinai, Egypt (northernmost Arabian–Nubian Shield). The Tarr carbonates are coarsely crystalline and related to explosive emplacement of hypabyssal and volcanic albitite at 605 ± 13 Ma. The carbonates associated with the albitites are divisible into two types: primary dolomitite and secondary breunneritite (Fe-rich magnesite). The dolomitite was clearly intrusive but differs from classic igneous carbonatites, containing much lower abundances of incompatible elements, such as REE, U, Th, Rb, Nb, Y, P, Sr, Zr, Ba, and total alkalis. The breunneritite is a secondary replacement of dolomitite, probably marking the roots of a vigorous hydrothermal system. Albitites show pristine abundances of major and trace elements and were not subjected to a major metamorphic overprint. They are relatively more fractionated, alkaline and related to within-plate A-type magmas, were emplaced in an extensional or non-compressive tectonic regime in the cupola of high-level A-type granite. Tarr albitites may represent residual magma remaining after near-total crystallization of an A-type granite pluton at depth, forcibly

emplaced into the roof above the cooling pluton. The intrusive dolomitite exsolved from highly differentiated albitite melt, in the apical regions of a still-buried alkaline “A-type” granite pluton that was rich in CO_2 ; these volatiles migrated upwards and towards the cooler margins of the magma body. Late NNE–SSW extension allowed a shallow-level cupola to form, into which albitite melts and carbonate fluids migrated, culminating in explosive emplacement of albitite breccia and intrusive carbonate. Isotopic compositions of Tarr dolomitite and albitite indicate these are consanguineous and ultimately of mantle origin. Magmatic volatiles fenitized the wall rock, while submarine hydrothermal activity transformed some of the dolomitite into breunneritite. Recognition of Tarr-type should encourage similar hypabyssal complex intrusions to be sought for in association with A-type granitic plutons elsewhere.

Keywords Albitite · Magmatic cupola · Intrusive dolomitite · Sr, Nd isotopes · Geochronology

Introduction

The basement rocks of Sinai lie at the northern end of the Arabian–Nubian Shield (ANS). The ANS is the northern part of the East African Orogen, which formed in Neoproterozoic time ($\sim 1,000$ – 542 Ma ago) by amalgamation of oceanic and continental magmatic arcs during subduction and obduction of oceanic crust and closure of the Mozambique Ocean (Kröner 1985; Kröner et al. 1987; Stern 1994; Loizenbauer et al. 2001). In the ANS, deformation and metamorphism were accompanied by the migration of carbonate-rich solutions (Stern and Gwinn 1990), veins and dikes of calcite and dolomite, less

M. K. Azer (✉)
Geology Department, National Research Centre,
Al-Behoos St., 12622-Dokki, Cairo, Egypt
e-mail: mokhles72@yahoo.com

R. J. Stern
Geosciences Department, University of Texas at Dallas,
Box 830688, Richardson, TX 75083-0688, USA

J.-I. Kimura
Institute for Research on Earth Evolution (IFREEE),
Japan Agency for Marine–Earth Science and Technology
(JAMSTEC), Yokosuka 237-0061, Japan

typically ankerite, magnesite, and breunnerite. The migration of these solutions also resulted in the diffuse and pervasive carbonation of a wide range of basement rocks. Although we are not yet able to quantify the volume of carbonate added to the crust of this region, it is clear that vast amounts of such fluids accompanied the greenschist-facies metamorphism of a large portion of the ANS. The source and age of this pervasive carbonate alteration in the ANS and in other Neoproterozoic is controversial but is important for understanding fundamental aspects of Earth evolution (Santosh and Omori 2008).

The present study contributes to this problem by studying the age, composition, and significance of an unusual body of intrusive carbonates associated with explosively emplaced albitite found in Wadi Tarr, southern Sinai. In spite of the fact that these are clearly intrusive and are carbonatites as defined by the IUGS classification (Streckeisen 1980), they are in many ways distinct from “classic” igneous carbonatites, especially in terms of containing much lower abundances of incompatible trace elements, such as REE, Nb, Sr, Zr, Ba, U and Th. In order to avoid confusion, we call the Tarr rocks “intrusive carbonates”.

There are relatively few studies of Neoproterozoic intrusive carbonates in Egypt, even though these are common in the Sinai Peninsula and the Eastern Desert. More studies have been done on Phanerozoic intrusive carbonates in the Eastern Desert, where El-Ramly et al. (1971) considered the intrusive carbonates associated with Phanerozoic ring complexes to be carbonatites, although the geochemical data indicate significant differences from “classic” mantle-derived carbonatites because they are depleted in Ba, Sr, Nb and REE. Carboniferous carbonate intrusions at Gebel Tarbti on the Red Sea coast of Egypt are considered as carbonatite (Serencsits et al. 1979; El-Haddad and Hashad 1984). Early Mesozoic intrusive carbonates associated with the Gebel Mansouri ring complex in the Eastern Desert of Egypt are considered to be carbonatites with peculiar trace element abundances (Hashad and El-Reedy 1980; El-Haddad et al. 1984; El-Nisr and Saleh 2001). They are characterized by low contents of Ba, Sr, Nb and REE, and isotopic data suggest a magmatic origin ($^{87}\text{Sr}/^{86}\text{Sr} = 0.7052$; Hashad 1981).

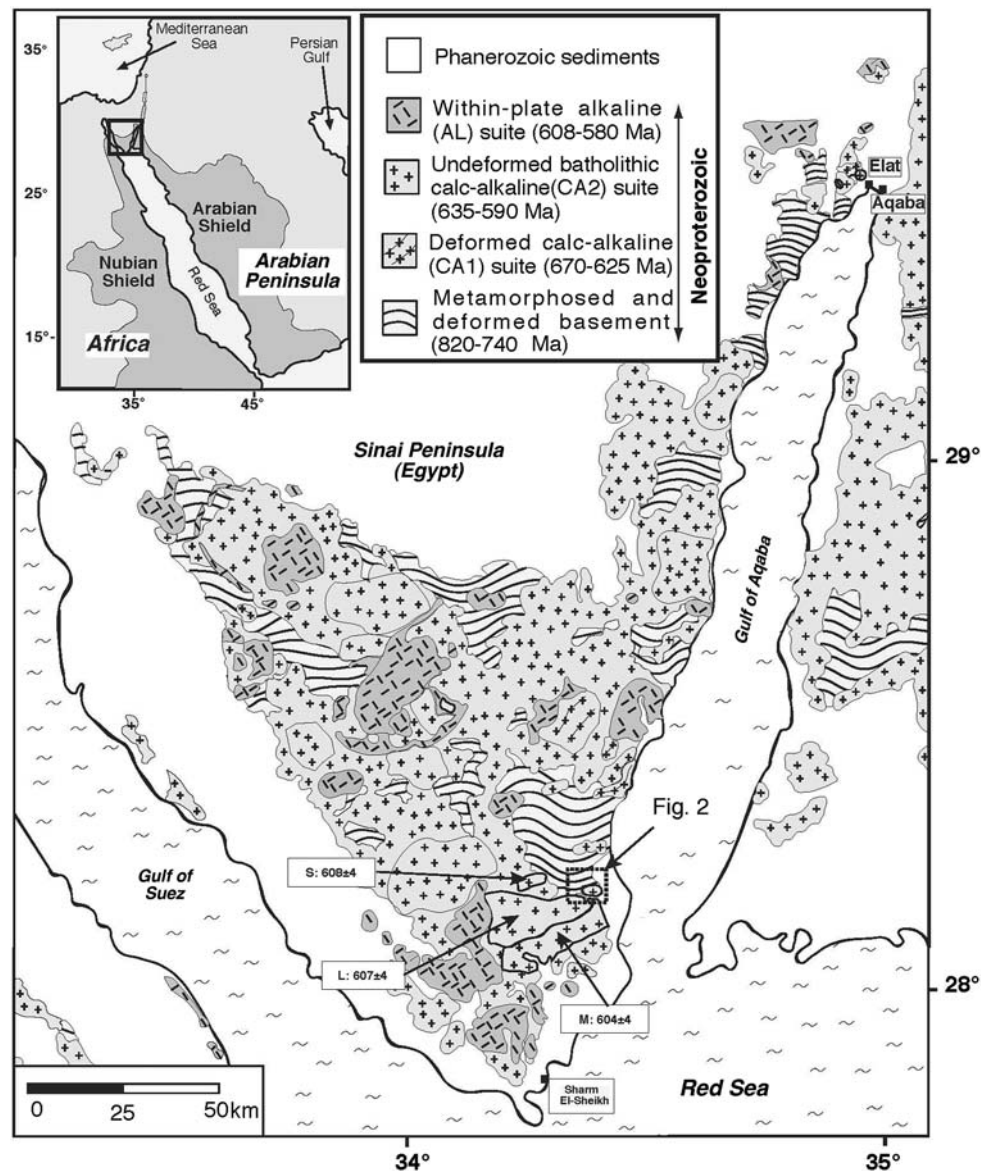
A regional study by Stern and Gwinn (1990) investigated the origin of Neoproterozoic intrusive carbonates in the Eastern Desert and NE Sudan, intruded as dikes and veins during Neoproterozoic time, but distinguished those from classic carbonatites because of their much lower contents of Sr compared to true carbonatite. Based on the isotopic data they distinguished the source of Neoproterozoic intrusive carbonates of the northern ANS into: (1) remobilized carbonate sediments, with moderately high $^{87}\text{Sr}/^{86}\text{Sr}$ (0.705–0.707) and heavy C ($\delta^{13}\text{C} = -2$ to $+4\%$)

and O ($\delta^{18}\text{O} = +15$ to $+25\%$), (2) fluids or melts derived from depleted mantle, with low $^{87}\text{Sr}/^{86}\text{Sr}$ (~ 0.7030) and light C ($\delta^{13}\text{C} = -8$ to -2%) and O ($\delta^{18}\text{O} = +6$ to $+10\%$), and (3) carbonatite melts derived from enriched mantle or lower crust with high $^{87}\text{Sr}/^{86}\text{Sr}$ (~ 0.71) and light C ($\delta^{13}\text{C}$ to -6%) and O ($\delta^{18}\text{O}$ to $+6\%$). On this basis, it appears that intrusive carbonates of the North Eastern Desert were derived from depleted mantle, whereas those of Central Eastern reflect mixing between remobilized sedimentary carbonates and mantle fluids. The low Sr contents led Stern and Gwinn (1990) to interpret the mantle-derived intrusive carbonates as having exsolved from cooling silicate melts rather than being derived directly from a carbonatitic mantle source.

An excellent example of Neoproterozoic intrusive carbonates is found at Wadi Tarr in southern Sinai (Fig. 1) associated with hypabyssal and volcanic albitite, which are together the focus of this study. Previous studies indicate that the carbonates are different than other igneous, metamorphic and sedimentary carbonates, stimulating controversy about their origin (Shimron et al. 1973; Bogoch et al. 1982, 1986; Blasy et al. 2001). Shimron (1975) suggested that the intrusive carbonates of Wadi Tarr are “atypical” carbonatites, resulting from an immiscible melt fraction separated from an albitite melt. Five papers by Bogoch in the 1980s highlighted the Tarr carbonates and albitite. Bogoch et al. (1982) agreed that the intrusive carbonates of Wadi Tarr were related to the albitite, and suggested derivation from a buried ophiolite; however, the presence of ophiolites in Sinai is doubtful (Bentor 1985; El-Gaby et al. 1990). Nevertheless, the intrusive carbonates show clear mantle affinities. Carbonate fluids and mantle-derived melts clearly co-existed, as demonstrated by carbonate-filled magmatic ocelli in associated diabase dikes (Bogoch and Magaritz 1983). Bogoch et al. (1984) attributed high Sc concentrations (30–150 ppm) in Tarr carbonate minerals to a mantle source. Bogoch et al. (1986) reported that the dolomite has H, O, C and Sr isotopic compositions consistent with a mantle source, while the isotopic composition of the breunnerite indicates re-equilibration of primary dolomite with metamorphic water to form breunnerite. Bogoch et al. (1987) interpreted the albitite as metasomatic in origin.

In this study, we present new field and geochemical data in order to determine the origin of the intrusive carbonates of Wadi Tarr and their relation to the albitites and sedimentary carbonates in the vicinity. We present new geochemical, isotopic, and geochronological data that allows a much broader perspective. We conclude that Tarr intrusive carbonates reflect processes in a high-level magmatic cupola and associated hydrothermal system, perhaps associated with a Neoproterozoic caldera complex above an A-type granite pluton.

Fig. 1 Simplified geological map of Neoproterozoic basement in and around Sinai, emphasizing the distribution of Ediacaran (Late Neoproterozoic) granitic rocks, modified after Be'eri-Shlevin et al. (2008b) in press). This map shows the location of the detailed study area shown in Fig. 2 and ages (in Ma) of nearby granitic rocks dated with U–Pb zircon ion probe techniques by Be'eri-Shlevin et al. (2008b) in press): S Sama pluton; L Lathi pluton, as well as the Mandahar pluton (M; Be'eri-Shlevin et al. 2008b). Note the similar ENE–WSW trend and indistinguishable age of these plutons to the age of the Tarr albitite determined here (605 ± 15 Ma). *Inset* shows the location of the Sinai in the northernmost ANS Neoproterozoic exposures of Eastern Africa and Western Arabia (dark gray)



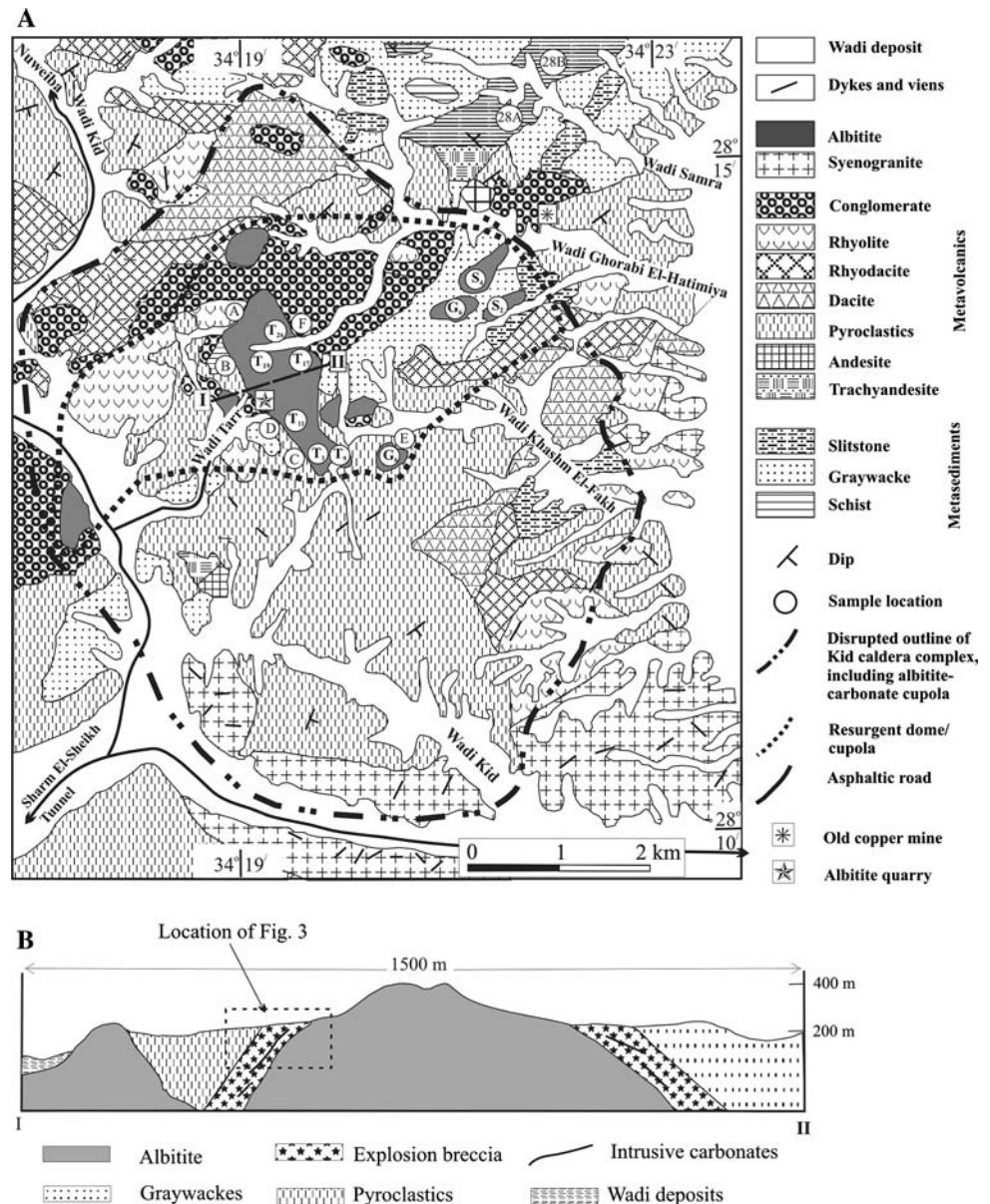
Geological setting

Exposed Neoproterozoic basement rocks in the Tarr area consist of metasediments, metavolcanics and pyroclastics, albitite, and syenogranite (Fig. 2a). The Tarr intrusive carbonate-albitite complex is found in the southernmost part of the Wadi Kid metamorphic core complex (Blasband et al. 1997, 2000). This core complex was active ~ 600 Ma ago, in association with strong NNW–SSE-directed extension in the northern ANS (Stern et al. 1984). The formation of core complex was accompanied by extensive magmatism and left-lateral strike-slip shearing on the Najd system (Stern 1985). Regional extension and shearing may manifest with the orogenic collapse of the northern ANS near the end of the Ediacaran.

The Kid metasediments are described by Shimron (1980) as having been deposited in a deep water environment. They consist of two well bedded, fining-upward successions of often laminated, porphyroblastic schists, mostly pelitic and interbedded with metacalpelites enclosing marble lenses, quartzites, as well as with metagreywackes, polymictic metaconglomerates, and porphyroblastic pebbly schists (Hafez et al. 2007). There are turbidities, with diagnostic sedimentary structures, such as fining-up sequences (Brooijmans et al. 2003). The carbonate metasediments including marble (Shimron 1975; Hafez et al. 2007) are particularly important for the present study.

Metavolcanic rocks include andesite, trachyandesite, dacite, rhyodacite, rhyolite, and associated pyroclastics, thought to have formed in an oceanic island arc (Shimron

Fig. 2 **a** Geological map of the Wadi Tarr area (after Blasy et al. 2001), **b** Geological cross section (I–II) showing the relationship between the intrusive carbonate and albitite of Wadi Tarr area



1980; Furnes et al. 1985; El-Metwally et al. 1999), geochemically similar to the calc-alkaline Younger Metavolcanics described by Stern (1981) in the Eastern Desert of Egypt. Other studies (El-Gaby et al. 1991; Moghazi 1994 and others) suggest that the Kid metavolcanics sequence may correlate with the subaerial calc-alkaline Dokhan Volcanics of the Eastern Desert of Egypt. In the latter case, the metavolcanic rocks may represent early stages in the magmatic evolution of the caldera complex we infer to be the setting of the Tarr intrusive carbonate–albitite complex. Field and geochronology studies are needed to resolve the significance of these metavolcanics.

The plutonic rocks in the Kid area include a gabbro-diorite complex (outside of Fig. 2a area) and various granitic bodies (Shimron 1980; Moghazi et al. 1998; Shahien

2002). The gabbro-diorite intrudes the volcano-sedimentary succession, but it is older than late- to post-tectonic granitoid intrusions. The granitoids are divided into three groups: (1) quartz-monzonite, (2) granodiorite-monzogranite, and (3) syenogranite (Iqna granite of Bielski et al. 1979) and albitite. Most of the granitic rocks are broadly A-type, late- to post-orogenic, typical of ~600 Ma plutons in the region (Jarrar et al. 2008; Be’eri-Shlevin et al. 2008b, in press), and include syenogranite and albitite. Three plutons in the immediate vicinity of the Tarr complex have been recently dated with modern U–Pb zircon techniques (Be’eri-Shlevin et al. 2008b), including the Lathi monzogranite (607 ± 4 Ma); the syenogranite in the SE corner of Fig. 2 is part of the Lathi pluton. Due west of the study area, the small Sama quartz monzonite–

monzogranite pluton gives a very similar age (608 ± 4 Ma). The Mandar pluton to the south of the Lathi pluton was dated using modern U–Pb zircon techniques by Be’eri-Shlevin (2008a) and yields an age of 604 ± 4 . It is worth noting that the 604 ± 4 Ma Mandar pluton was previously dated as 530 Ma by Rb–Sr techniques (Bielski 1982).

Albitite is exposed along and east of the asphaltic road in Wadi Kid, especially in Wadi Tarr (Fig. 2a). The Tarr albitites occur as small (<1.2 km²) intrusions associated with widespread brecciation and alteration of the surrounding country rocks, and with small bodies of intrusive carbonates as well as olivine dolerite and lamprophyre dykes. Albitite masses were intruded into the metavolcanic–metasedimentary units and about ten albitite bodies define a zone that trends NE, approximately paralleling extensional dike swarms and the long axis of the Kid core complex. Albitite bodies are surrounded by breccia zones, about 100–150 m wide (Figs. 2b, 3). The breccia is very coarse (fragments are a few centimeters to 10 m across) and can be subdivided into interior and exterior zones. Interior breccia zones consist of angular fragments of brown albitite or country rock in a groundmass of pale yellow prismatic to fibrous actinolite. Exterior breccia zones consist of angular fragments of country rocks, mainly metatuffs, cemented by coarse intrusive carbonate. The angularity of clasts and absence of foreign fragments imply that they formed in situ. The breccia is interpreted as related to emplacement of the albitite and indicates violent, even explosive, emplacement perhaps due to volatile overpressure. Locally, the silicate rocks within the breccia zone are strongly amphibolitized; this alteration locally extends away from the stocks into the non-brecciated country rocks (Bentor and Eyal 1987), defining a zone of fenitization (Shimron 1975). Original K-feldspars in the wall rock are converted to albite, turbid with sericite. Plagioclase is converted to fine sericite–calcite aggregates with clear patches of albite. New crystals and nests of albite and phlogopite are observed in the metatuffs.

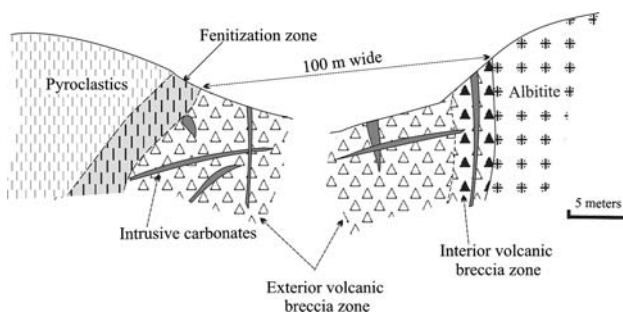


Fig. 3 Sketch showing the relationship between the intrusive carbonate–albitite complex and their country rocks

The intrusive carbonates of Wadi Tarr were emplaced around some (but not all) and locally within the albitites (Fig. 2b). Rarely, the carbonates intrude the surrounding metasediments. Intrusive carbonates are represented by dolomitite, sometimes replaced by brunneritite. They occur as veins and dyke-like bodies (several centimeters up to 1 m wide) and as subhorizontal sheets (3–10 m thick and up to 150 m long). They also occur as cement in the albitite breccia. On fresh surfaces, the dolomitite is white to light grey and the brunneritite is medium to dark brown; both minerals weather dark beige.

The Tarr intrusive carbonate–albitite complex and possible caldera developed in association with profound lithospheric thinning, as shown by coexistence with the Tarr metamorphic core complex. Field evidence shows that the intrusive carbonate–albitite complex is younger than other Neoproterozoic rocks in the vicinity. The intrusive carbonates were emplaced contemporaneous with or slightly later than the albitite. The only published geochronology is fission track dating of epidote in the albitite, which gave an Early Cretaceous age [103 ± 8.3 Ma; Barr (1973) cited in Bentor and Eyal (1987)].

Analytical techniques

Powdered samples of intrusive dolomitite, brunneritite, and sedimentary carbonates were subjected to X-ray diffraction analysis to determine their mineralogy. The powder diffraction pattern of the samples was obtained with Cu radiation with secondary monochromator. The scanning speed was $2\theta = 1^\circ/\text{min}$ at constant voltage 40 KV and 40 mA using BRUKER D₈ advanced X-ray diffractometer at the Central Metallurgical and Development Institute in Cairo. Mineral identification was carried out using the data given in the American Standard Test Materials (ASTM) cards by measuring the *d*-values of the different atomic planes and their relative intensities.

Polished thin sections of selected intrusive dolomitite and brunneritite were examined with a Philips XL30 environmental scanning electron microscope (ESEM) at the Nuclear Materials Authority in Egypt, operating at 25 KV and equipped with EDAX energy dispersive analytical X-ray spectrometer. The spectrometer detects elements with atomic number >4 (B and heavier elements), with counting rates kept close to 1,000–1,500 counts per second. ESEM analyses (normalized to 100%) are listed in Table 1.

Geochronology involved separating zircons and analyzing them with an ion probe. Heavy minerals were separated from albitites at NRC and further purified at UTD. Separated zircons were mounted into a 25 mm epoxy puck along with the 1,065 Ma Geostandards 91500

Table 1 ESEM mineral compositions of the intrusive dolomitite and breunneritite (normalized to 100%)

Sample Spot No.	Dolomitite (100C)			Breunneritite (200C)			
	1	2	3	1	2	3	4
SiO ₂	0.00	0.02	0.36	0.83	0.34	1.06	0.98
Al ₂ O ₃	0.02	0.00	0.51	0.00	0.00	0.38	0.47
Fe ₂ O ₃	5.81	6.11	5.74	17.52	16.38	18.34	19.56
MnO	0.68	0.71	0.46	0.63	0.56	0.54	0.59
MgO	24.96	21.22	22.98	30.95	29.24	28.10	29.61
CaO	26.66	27.52	25.78	8.77	7.41	9.02	9.43
P ₂ O ₅	0.10	0.00	0.21	0.11	0.08	0.29	0.18
CO ₂	41.77	44.42	43.96	41.19	45.99	42.27	39.18
Total	100.00	100.00	100.00	100.00	100.00	100.00	100.00

reference zircon (Wiedenbeck et al. 1995) and polished approximately half-way through. Preanalytical cathodoluminescence images were obtained using a Hitachi S4300 scanning electron microscope equipped with a Gatan “mini-CL” detector at the Swedish Museum of Natural History. Following CL imaging, samples were coated with ca. 30 nm of gold.

Secondary ion mass spectrometer (SIMS) U–Th–Pb analyses were carried out using a large geometry Cameca IMS1270 instrument at the Swedish Museum of Natural History. Instrument set up broadly follows that described

by Whitehouse et al. (1999) and Whitehouse and Kamber (2005), using a ca. 15–20 μm O₂[−] primary beam with 23 kV incident energy. A mass resolution (M/ΔM) of ca. 5,400 was used to ensure adequate separation of Pb isotope peaks from nearby HfSi⁺ species. Presputtering, secondary ion beam centering, mass calibration optimisation, and adjustment of the secondary beam energy distribution were performed automatically for each run and runs were combined in an automated chain sequence. Data reduction assumes a power law relationship between Pb⁺/U⁺ and UO₂⁺/U⁺ ratios to calculate actual Pb/U ratios based on those in the 91500 standard. U concentrations and Th/U ratio are also referenced to the 91500 standard. Common Pb corrections are made only when ²⁰⁴Pb counts statistically exceed average background and assume a ²⁰⁷Pb/²⁰⁶Pb ratio of 0.83 (equivalent to present day Stacey and Kramers (1975) model terrestrial Pb). Age interpretations use the routines of Isoplot/Ex (Ludwig 2001). Decay constants follow the recommendations of Steiger and Jäger (1975) (Table 2).

Three representative samples of the intrusive dolomitite, three samples of the breunneritite and ten samples of the albitite as well as two samples of sedimentary carbonates were analyzed for major and trace elements using X-ray fluorescence spectrometry (XRF). The XRF analyses were carried out at Shimane University in Japan and at the Saudi Geological Survey, Jeddah, Saudi Arabia. Loss on ignition

Table 2 Ion microprobe U–Th–Pb analytical data and derived ages for Tarr albitite rocks, Egypt

Spot	No. scans	f ²⁰⁶ Pb† (%)	U (ppm)	Th (ppm)	Pb (ppm)	²⁰⁶ Pb/ ²³⁸ U	±σ (%)	²⁰⁷ Pb/ ²⁰⁶ Pb	±σ (%)	²⁰⁷ Pb/ ²³⁵ U age (Ma)	²⁰⁶ Pb/ ²³⁸ U age (Ma)	²⁰⁷ Pb/ ²⁰⁶ Pb age (Ma)
1	12	0.21	90	62	11	0.1003	1.42	0.0587	2.06	611 ± 12	616 ± 8	593 ± 44
2	12	0.59	73	34	9	0.0974	2.17	0.0575	2.84	581 ± 16	599 ± 12	510 ± 61
3	12	0.33	101	67	13	0.1039	1.41	0.0586	1.94	619 ± 11	637 ± 9	553 ± 42
4	12	2.31	570	397	63	0.0915	1.42	0.0609	2.08	578 ± 11	564 ± 8	635 ± 44
5	12	1.19	561	320	60	0.0929	1.41	0.0598	1.33	577 ± 9	573 ± 8	595 ± 29
6	12	0.16	143	35	16	0.1009	1.42	0.0584	1.43	604 ± 9	620 ± 8	546 ± 31
7*	12	7.88	1084	835	86	0.0646	1.46	0.0607	3.11	439 ± 12	404 ± 6	628 ± 66
8	12	1.13	370	253	43	0.0959	1.45	0.0597	1.59	591 ± 10	590 ± 8	592 ± 34
9	12	0.07	551	98	62	0.1003	1.41	0.0603	0.73	616 ± 7	616 ± 8	614 ± 16
10	12	0.11	118	23	13	0.1019	1.45	0.0593	1.76	616 ± 11	626 ± 9	579 ± 38
11	12	0.07	692	156	80	0.1021	1.44	0.061	0.59	629 ± 7	627 ± 9	639 ± 13
12	12	0.15	122	85	15	0.0969	1.41	0.0596	1.55	595 ± 10	596 ± 8	590 ± 33
13	12	0.06	314	77	35	0.099	1.46	0.0603	1.02	610 ± 8	608 ± 9	613 ± 22
14	12	0.06	185	128	24	0.1011	1.42	0.0603	1.15	619 ± 9	621 ± 8	614 ± 25
15*	12	29.64	1,585	2,121	16	0.0158	1.76	NA	NA	NA	101 ± 2	NA
16	12	0.07	191	151	25	0.1001	1.44	0.0597	1.18	611 ± 9	615 ± 9	593 ± 25
17	12	0.07	269	185	34	0.0992	1.42	0.0593	1	603 ± 8	610 ± 8	578 ± 22
18*	12	1.86	911	375	95	0.0886	1.42	0.0601	2.55	559 ± 13	547 ± 8	607 ± 54
19*	12	3.13	1,215	1,124	78	0.0604	1.45	0.0582	1.98	402 ± 8	378 ± 5	539 ± 43
20*	12	0.28	1,187	541	103	0.0731	1.42	0.0605	0.97	484 ± 7	455 ± 6	622 ± 21

*Indicates data excluded from calculated age

Table 3 Chemical compositions of intrusive dolomitite, breunneritite and sedimentary carbonates

Sample	Dolomitite			Breunneritite			Sedimentary carbonates	
	100A	100B	100C*	200A	200B	200C*	28A*	28B*
SiO ₂	0.00	0.00	0.00	1.59	0.56	0.00	0.00	0.00
TiO ₂	0.00	0.00	0.00	0.02	0.00	0.02	0.02	0.03
Al ₂ O ₃	0.09	0.10	0.15	0.11	0.01	0.57	0.51	0.55
Fe ₂ O ₃	3.51	4.08	4.58	17.26	12.76	12.82	0.96	0.85
MnO	0.46	0.49	0.47	0.32	0.23	0.25	1.49	0.91
MgO	29.01	26.82	22.17	27.07	34.60	30.67	7.10	2.31
CaO	24.06	23.06	26.79	10.82	5.69	12.41	47.09	53.71
Na ₂ O	0.00	0.02	0.01	0.03	0.01	0.04	0.00	0.00
K ₂ O	0.01	0.03	0.05	0.00	0.01	0.05	0.00	0.00
P ₂ O ₅	0.00	0.00	0.00	0.00	0.00	0.05	0.03	0.03
L.O.I	43.05	45.01	45.79	42.11	45.19	43.12	42.80	41.60
Total	100.19	99.61	100.00	99.33	99.06	100.00	100.00	99.99
Trace element in raw samples (ppm)								
Ba	35	31	31	46	37	39	23	14
Cr	81	116	112	198	79	89	4	6
Ga	n.d	n.d	0	n.d	n.d	1	0	0
Nb	<10	<10	0	<10	<10	1	1	1
Ni	26	61	37	271	117	167	10	5
Rb	<20	<20	0	<20	<20	1	1	0
Sr	198	207	237	101	129	109	136	112
Th	n.d	n.d	2	n.d	n.d	1	5	5
V	58	66	44	104	131	94	33	33
Y	19	22	26	4	6	2	4	4
Zr	<20	<20	5	<20	<20	7	14	13

*Indicates samples analyzed at Shimane U., others analyzed at Saudi Geological Survey, Jeddah, Saudi Arabia

(L.O.I.), for the samples analyzed in Saudi Arabia was determined by heating powdered samples for 1 h at 1,000°C. The XRF analyses were carried out at Shimane University on glass discs (flux-to-sample ratios of 2:1) for both major and trace elements (Kimura and Yamada 1996) and at the Saudi Geological Survey on fused-glass discs for major and pressed-powder pellets for trace elements. XRF analyses are listed in Tables 3 and 5.

Trace element concentrations (including the REE) were determined for nine samples (1 dolomitite, 1 breunneritite, 2 sedimentary carbonates, and 5 albitites) at Shimane University, following the methods of Kimura et al. (1995, 2002). Acid reagents used were EL-grade nitric (Kanto Chemicals) and hydrofluoric acid (Tama Chemicals), and analytical grade perchloric acid (Wako Chemicals). Experimental water was distilled and subsequently ion exchanged with a Milli-Q filter (Millipore). Procedural blanks were <1 ppt. The ICP-MS system used was a Thermo ELEMENTAL VG PQ3 equipped with a normal concentric nebulizer and a water-chilled impact bead-type nebulizer. Instrument settings were fundamentally those of

Kimura et al. (1995). Analytical precision is better than 2% and external analytical reproducibility better than 6% by repeated analyses over 10 years. ICP-MS analyses are listed in Tables 4 and 6.

Analytical procedures for Sr and Nd isotope separations follow Iizumi et al. (1994, 1995). Reagents were Ultrapur grade hydrofluoric and nitric acids (Merck), and precise measurement grade hydrochloric acid (Wako Chemicals). Distilled deionized water and hydrochloric acid were simmered before use, and procedural blanks were <1 pg/g for both Nd and Sr. Samples were analyzed by VG Elemental Plasma 54 Multiple Collector-Inductively Coupled Plasma-Mass Spectrometer (MC-ICP-MS) at Shimane University, for both Nd and Sr using Aridus desolvating nebulizer. NIST SRM987 Sr standard and La Jolla Nd standard were analyzed before and after unknowns. Standard values (and 2σ errors) during the analyses were $^{87}\text{Sr}/^{86}\text{Sr} = 0.710244 \pm 0.000020$ ($n = 4$) and $^{143}\text{Nd}/^{144}\text{Nd} = 0.511866 \pm 0.000010$ ($n = 4$), respectively. Typical internal 2 standard errors (2SE) for sample analyses are ± 0.000015 for Sr and ± 0.000010 for Nd. Isotope analyses are listed in Tables 7 and 8.

Table 4 REE and some trace elements by ICP-MS in the carbonate rocks

Sample	Breunneritite		Sedimentary carbonates	
	Dolomitite 100C	200C	28A	28B
La	18.60	0.45	3.01	2.07
Ce	46.75	1.21	5.25	3.92
Pr	5.56	0.22	0.65	0.55
Nd	23.99	1.16	2.72	2.05
Sm	4.69	0.45	0.58	0.45
Eu	1.71	0.14	0.14	0.12
Gd	4.29	0.59	0.71	0.53
Tb	0.61	0.10	0.10	0.09
Dy	3.64	0.56	0.56	0.50
Ho	0.67	0.11	0.12	0.11
Er	1.70	0.30	0.33	0.30
Tm	0.25	0.05	0.05	0.05
Yb	1.67	0.47	0.34	0.33
Lu	0.25	0.09	0.06	0.06
∑REE	114.38	5.89	14.60	11.14
(Eu/Eu*)	1.16	0.82	0.66	0.72
(La/Lu) _n	7.89	0.52	5.46	3.53
(La/Sm) _n	2.56	0.65	3.35	2.95
(Gd/Lu) _n	2.10	0.78	1.50	1.04
Li	1.102	1.337	3.131	4.893
Be	0.128	0.173	0.166	0.079
Rb	0.105	0.123	0.016	0.012
Y	17.707	2.626	4.621	3.635
Zr	0.467	4.842	5.717	5.549
Nb	0.029	0.245	0.257	0.284
Sb	0.212	0.151	0.041	0.057
Cs	0.034	0.018	0.017	0.013
Ba	14.189	11.879	30.570	15.152
Hf	0.010	0.129	0.077	0.103
Ta	0.001	0.016	0.013	0.022
Tl	0.001	0.006	0.019	0.014
Pb	1.564	1.301	0.301	0.243
Th	0.197	0.100	0.128	0.133
U	0.030	0.275	2.407	1.674

Petrography and mineralogy

Intrusive carbonates

Two types of intrusive carbonate are associated with the albitite: primary dolomitite, and secondary breunneritite (Fe-rich magnesite). The term breunnerite was first used by Haidinger (1825; in Palache et al. 1951) to describe a magnesite containing 8 to 17 wt% FeCO₃. A more recent definition of breunnerite is that this contains 5–50 wt% FeCO₃ (Deer et al. 1992). Dolomitite is more abundant than the breunneritite among Tarr intrusive carbonates.

Dolomitite consists mainly of dolomite with minor amounts of calcite. Dolomite is white to light grey, and occurs as coarse (grains = 0.5–4.0 cm) and fine-grained (<0.5 cm) aggregates, sometimes showing pressure twinning. Some dolomitite contains large, subrounded dolomite crystals up to 4 cm long that are enclosed in a fine-grained groundmass showing mosaic texture (Fig. 4a). The large crystals are interpreted as phenocrysts, whereas the fine-grained groundmass may be recrystallized. A few phenocrysts are zoned, with clear cores and spongy, limonitized rims. Secondary quartz is observed as thin veins cutting carbonate minerals. Accessory minerals in the intrusive dolomitite are iron oxides, chlorite, talc, actinolite, and apatite. The breunneritite is coarse-grained, medium to dark brown, and consists mainly of coarse rhombohedra of breunnerite (0.5–5.0 cm) with minor tremolite. Secondary iron oxides give a dark brown color around rhomb boundaries and along cleavage planes (Fig. 4b). Flattened fibers of brown iron oxides penetrate the carbonate minerals and coalesce into larger masses. Rarely, serpentinized mafic minerals are observed in the breunneritite (Fig. 4c). Sometimes, fine-grained breunnerite can clearly be observed to have formed at the expense of primary dolomite. Sometimes the breunnerite is replaced by Fe–Mn oxides.

X-ray diffraction patterns for the dolomitite indicate that this is mostly ferroan dolomite (ankerite), with minor chabazite and magnesite. Breunneritite consists mainly of magnesite together with ferroan dolomite (ankerite). Quartz and kaolinite are also rarely observed in the breunneritite. Comparison of chemical compositions of dolomitite and breunneritite determined by ESEM (Table 1) indicates that replacement of dolomite involved massive loss of CaO and gain of FeO; there is also modest gain of MgO.

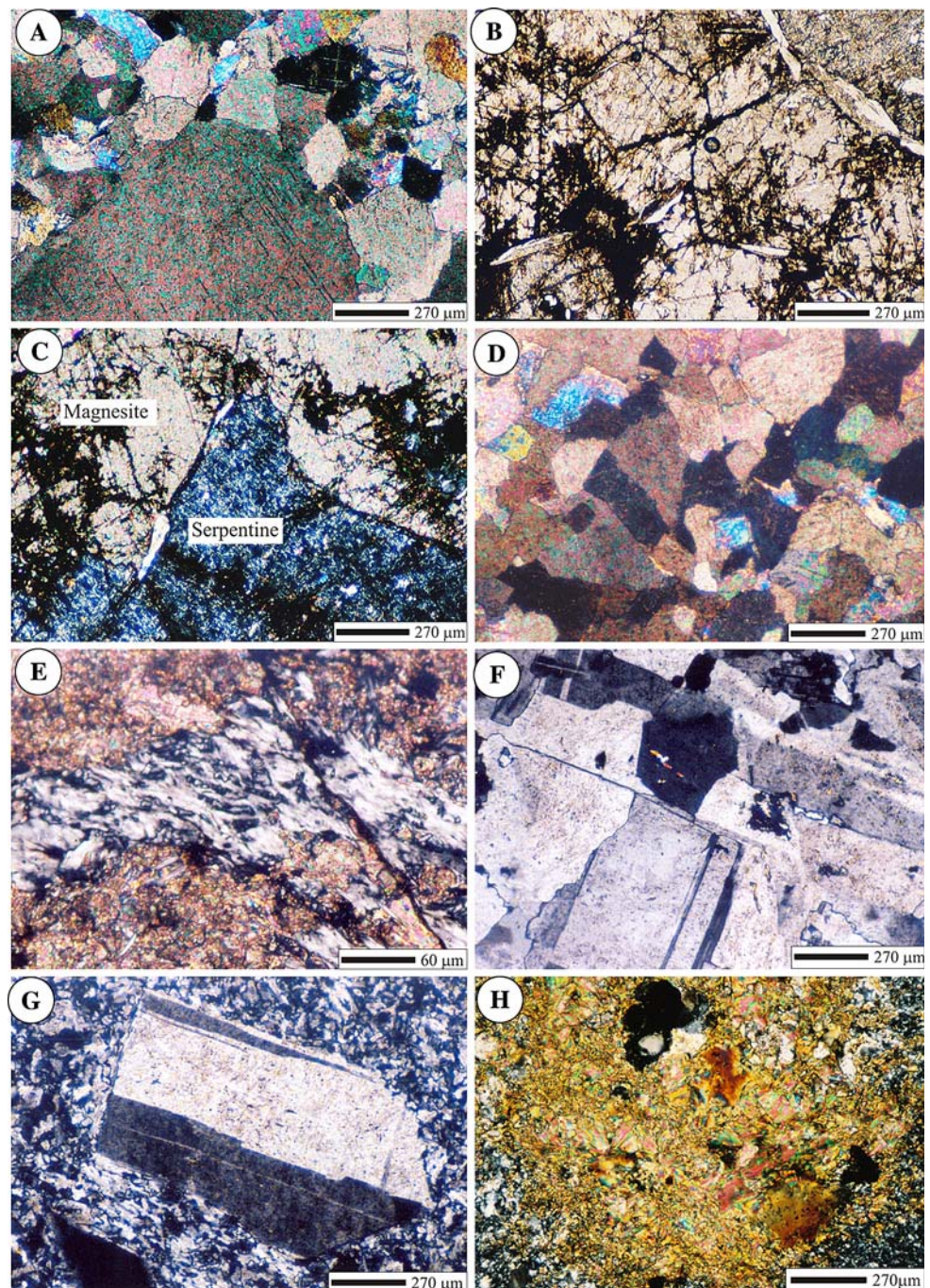
Sedimentary carbonates

Sedimentary carbonates are subdivided into recrystallized limestone (marble) and micritic limestone (lime mudstone). X-ray diffraction patterns indicate that these consist mainly of calcite and dolomite as well as less amounts of kaolinite and montmorillonite. Marble consists of sutured crystals of dolomite and calcite showing mosaic texture (Fig. 4d), while the micritic limestone is fine-grained and consists mainly of calcite, dolomite, and kaolinite showing recrystallization in some parts. The micritic limestone contains microveins of fibrous or platy serpentine (Fig. 4e) and chlorite–serpentine intergrowths (septechlorites). Periclase and tremolite pods are rarely observed within the sedimentary carbonates.

Albitite

The albitite is a leucocratic, pale yellow to white or light grey, fine- to medium-grained rock. The western albitites

Fig. 4 **a** Large crystals of dolomite enclosed in recrystallized fine-grained groundmass in the dolomitite (sample 100C), **b** Secondary iron oxides outlining carbonate rhomb boundaries and along cleavage planes of breunnerite (sample 200C), **c** Serpentinized mafic minerals in the breunnerite (sample 200B), **d** Recrystallized sedimentary limestone showing mosaic texture (sample 28A), **e** Serpentine minerals in micritic sedimentary limestone (sample 28B), **f** Medium-grained albitite with equigranular texture (sample T₂₆), **g** Porphyritic albitite containing phenocrysts of albite in a groundmass chiefly consisting of albite (sample S₄), and **h** Secondary biotite and muscovite nests in the fenitization zone in the wallrocks (sample 130)



(Wadi Tarr) are generally medium-grained with equigranular texture (Fig. 4f) and are thought to be subvolcanic (hypabyssal), whereas the eastern albitites (Wadi Ghorabi El-Hatimiya and Wadi Khashm El-Fakh) are fine-grained, porphyritic (Fig. 4g) and probably volcanic. In the porphyritic varieties, tabular subhedral to euhedral albite crystals up to 3 mm long are set in a fine-grained groundmass made up of an interlocking mosaic or of subhedral microlites of albite. Rarely, the groundmass shows spherulitic texture. In both types, albite accounts for 76–90%, quartz 3–11%, and orthoclase <5%. Accessory minerals are zircon, sphene,

apatite, biotite, and iron oxides, whereas secondary minerals include chlorite, muscovite, and actinolite. Albitite is highly sheared along faults, showing cataclastic texture.

Breccia and alteration zone

The volcanic breccia around the albitites is composed mainly of angular to subrounded rock fragments and blocks embedded in tuffaceous or carbonate groundmass. The rock fragments consist mainly of albitite, slate, and metavolcanics. Near some—but not all—of the albitites, new

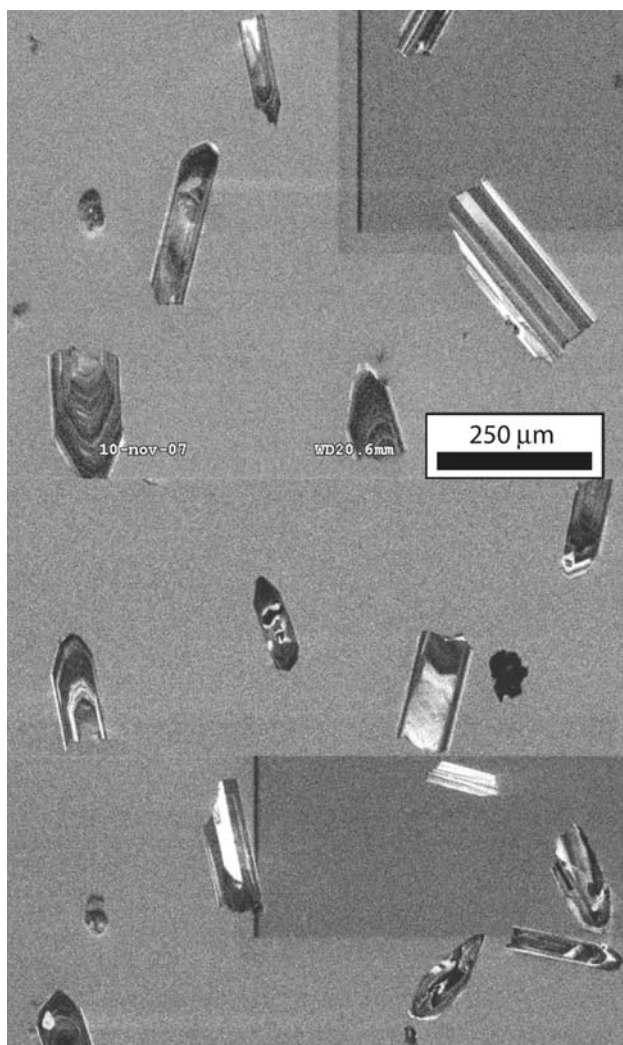


Fig. 5 Cathodeluminescence images of zircons extracted from Tarr albitites

minerals such as phlogopite, muscovite, biotite, albite and rare amphibole are developed in a narrow zone (~10–30 m wide). The new minerals occur in nests (Fig. 4h) and may be related to metasomatic processes (fentization). Tectonic origin of the breccia cannot be precluded entirely due to the presence of large number of faults in the vicinity which cross the albitite masses.

Geochronology

Zircons separated from albitite appeared euhedral, well-zoned, and entirely of magmatic origin (Fig. 5). No cores were observed. Analyses were attempted on 20 zircons (Table 2). One of these did not produce an age and four others were discarded because they were discordant or contained high U contents (>900 ppm). The 15 remaining analyses yielded a concordia age of 605 ± 13 Ma (Fig. 6),

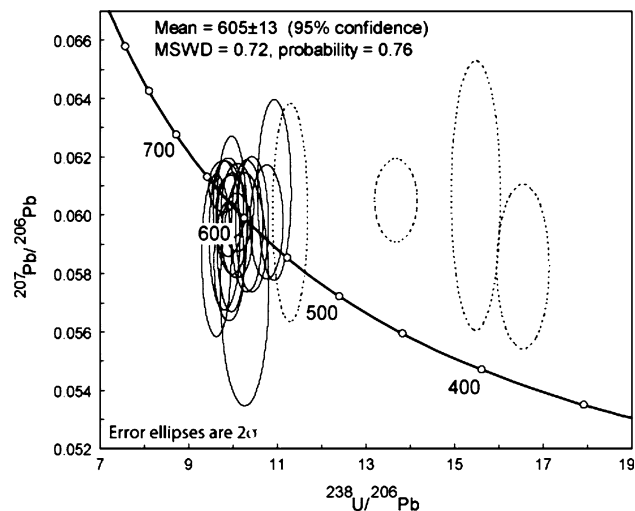


Fig. 6 Tera-Wasserburg U–Pb Concordia diagram for zircons from Tarr albitites. Note that age is defined using 15 of 20 points analyzed the other five points were rejected because they contain high U contents or were discordant, probably indicating significant Pb loss

interpreted as the crystallization age of the albitite and the age of carbonate intrusion. This age also indicates that intrusion and cooling of the albitite was synchronous with 590–605 Ma A-type granites of the Eastern Desert of Egypt (Moussa et al. 2008; Andresen et al. (2008)) and 593 ± 16 Ma (Rb–Sr whole rock age) for the Katherina Ring Complex (Katzir et al. 2007).

Geochemistry

Intrusive carbonates

Chemical analyses of the intrusive and sedimentary carbonates are listed in Table 3. The intrusive carbonates generally contain low Na, K, Rb, Sr, Ba, Nb, Y, Zr, Th, and REE contents compared to “classic” carbonatites. Compared to the breunneritite, the intrusive dolomitite is rich in Ca, Sr, Y, and REE and depleted in Fe, V, and Ni. The breunneritite contains 12.8–17.3 wt% Fe_2O_3 . The dolomitite contains much more Ca than the breunneritite and correspondingly higher concentrations of Sr, Y, and REE. The breunneritite contains slightly more Mg and Fe, thus correspondingly higher concentrations of Ni and V, than the dolomitite. Dolomitite and breunneritite contain similar contents of those trace elements that do not easily substitute for Mg or Ca, such as Ba, Pb, and Cr. The intrusive dolomitite and breunneritite contain low concentrations of high-field strength elements Nb, Ta, Zr, Hf, U, and Th, but the breunneritite contains more Nb, Ta, Zr, Hf, and U, whereas the dolomitite contains more Th. Our data confirm the observation of Bogoch et al. (1986) that the dolomitite contains more REE than the breunneritite. Both dolomitite

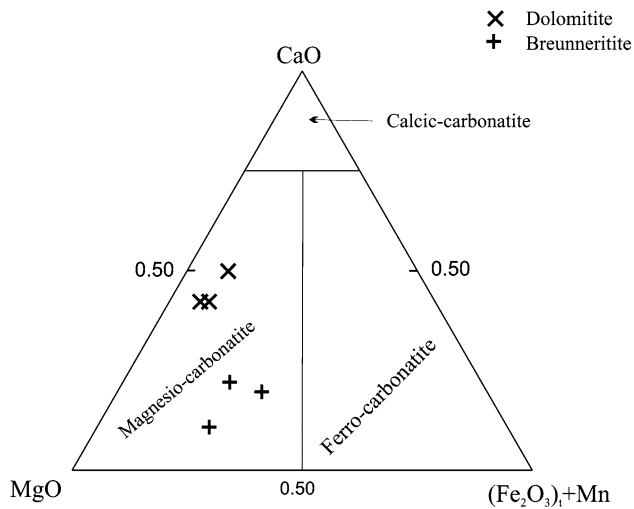


Fig. 7 Chemical classification of carbonatites, showing that Tarr intrusive dolomitite and breunneritite are magnesio-carbonatite (Woolley and Kempe 1989)

and breunneritite contain much more FeO, MgO, Ba, Cr, Ni, and V than do the sedimentary carbonates.

It is difficult to classify the Tarr intrusive carbonates consistently using existing classification schemes. A similar problem confronted the regional study of Stern and Gwinn (1990). Contrasting views about the origins of carbonatites were summarized by Gittins (1989) who noted, “No clear picture has emerged of what carbonatite magmas are, what chemical composition they have, where they develop, and how they evolve.” Carbonatite is defined in the IUGS system of classification as an igneous rock composed of more than 50 modal% primary (magmatic) carbonate and containing less than 20 wt% SiO₂ (Le Maitre 2002). By this definition, the Tarr intrusive carbonates are clearly carbonatite. The IUGS scheme subdivides carbonatites according to mineralogical or chemical composition (Woolley and Kempe 1989). Mineralogically, Tarr intrusive dolomitite is dolomite–carbonatite. On the CaO–MgO–(FeO + Fe₂O₃ + MnO) ternary diagram, the intrusive carbonates of Wadi Tarr are magnesio-carbonatite (Fig. 7).

Some workers restrict the term carbonatite to intrusive carbonates that are enriched in trace elements. Indeed, carbonatite rocks are economically important because they contain high concentrations of REE, Nb, Ta, U, and Th. According to Samoilov (1991), carbonatites are enriched in Sr (>700 ppm), Ba (>250 ppm), V (>20 ppm), REE including Y (>500 ppm), and LREE relative to HREE and Y. The low contents of Sr, Ba, Nb, Y, Th, and REE eliminate Tarr intrusive carbonates as carbonatites as characterized by Le Bas (1981). Also, true carbonatites contain significant Nb, P, Ta, Zr, and occasionally Zn and Pb. On the trace element discrimination diagrams of Samoilov (1991), the Wadi Tarr intrusive carbonates plot in the fields of sedimentary and metamorphic carbonate

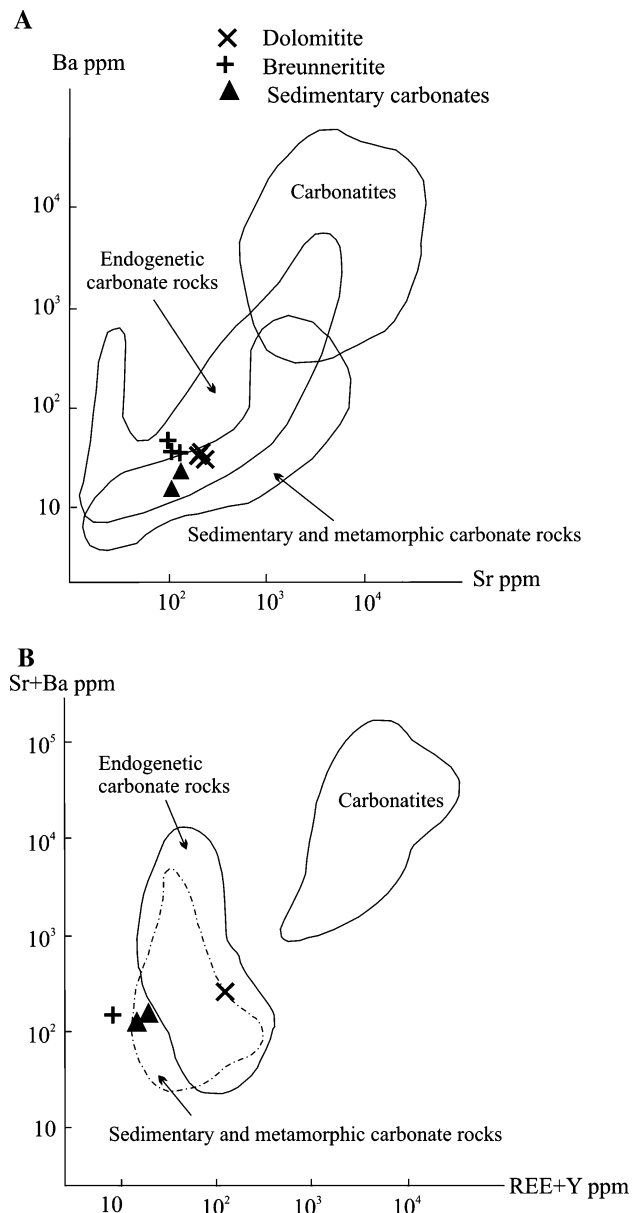


Fig. 8 a Diagram of Sr versus Ba (Samoilov 1991) for carbonatite, sedimentary, metamorphic and endogenic carbonate rocks, **b** Diagram of Sr + Ba versus REE + Y (Samoilov 1991) for carbonatite, sedimentary, metamorphic and endogenic carbonate rocks

rocks as well as endogenic (intrusive) field, but not in the field of carbonatites (Fig. 8a, b).

Representative REE analyses of Tarr intrusive and sedimentary carbonates are listed in Table 4. The intrusive dolomitite contains much higher REE contents than the breunneritite. The different REE profiles of the intrusive dolomitite and breunneritite (Fig. 9a) suggest different origins. The intrusive dolomitite is light REE enriched, whereas the breunneritite has a nearly flat REE pattern, with greater depletion of the light REE than the heavy REE. REE

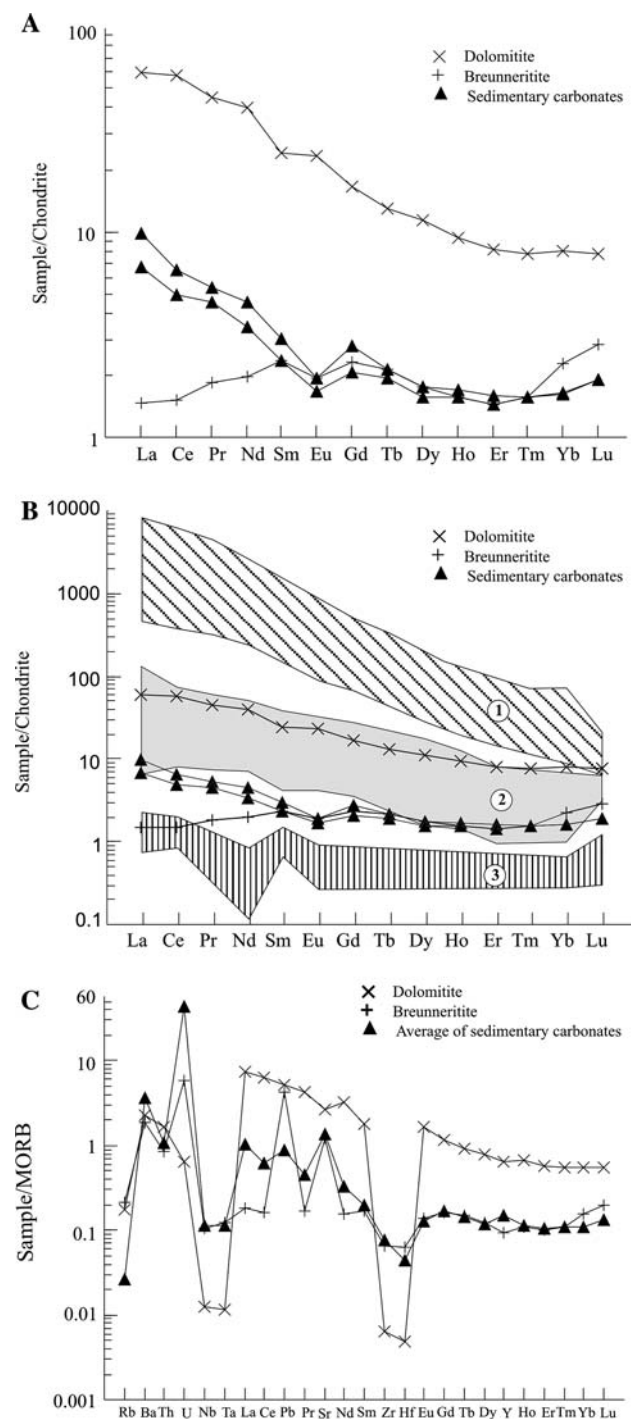


Fig. 9 **a** Rare-earth elements of the intrusive dolomitite, breunneritite, and sedimentary carbonates of Wadi Tarr normalized to chondrite (Boynnton 1984), **b** Comparison of Wadi Tarr intrusive dolomitite and breunneritite with other intrusive carbonates (using the chondrite values of Boynnton 1984): (1) Classic igneous carbonatite (Woolley and Kempe 1989; Wagner et al. 2003; Brassinnes et al. 2005; Srivastava et al. 2005b), (2) Mantle-derived dolomitite of SE Zimbabwe (Harmer et al. 1998), and (3) Intrusive carbonates of ring complexes in the Eastern Desert of Egypt (El-Haddad et al. 1984), and **c** MORB-normalized spider diagram for the intrusive dolomitite, breunneritite, and sedimentary carbonates. Normalization values are taken from Pearce and Parkinson (1993)

abundances for the breunneritite are more similar to the sedimentary carbonates in the area, except containing less La, Ce, Pr and Nd.

It is clear that the Tarr intrusive dolomitite has lower REE contents than classic carbonatites (Fig. 9b), but it is similar to the mantle-derived dolomitite carbonatites of SE Zimbabwe (Harmer et al. 1998). Moreover, intrusive carbonates with low REE abundances have been found in Italy (Castorina et al. 2000), south India (Srivastava et al. 2005a), the eastern Himalayan syntaxis (Liu et al. 2006), and the Gebel Mansouri ring complex in the Eastern Desert of Egypt (El-Haddad et al. 1984).

Sedimentary carbonates

Compared to the intrusive carbonates, the sedimentary carbonates are rich in MnO and CaO, and depleted in Fe₂O₃, MgO, Ba, Cr, Ni, and V. Sedimentary carbonates have Y and Sr contents that are similar to those of breunneritite but lower than abundances in the intrusive dolomitite. On the discrimination diagrams for carbonate rocks, the metamorphosed sedimentary carbonates of Wadi Tarr plot within fields for sedimentary and metamorphic rocks as well as in endogenetic (intrusive) fields (Fig. 8a, b). The REE patterns of the sedimentary carbonates parallel each other, with slightly negative Eu anomalies, thus differing from the intrusive carbonates. The geochemical characteristics of the sedimentary carbonates are similar to breunneritite.

A MORB-normalized multi-element diagram for intrusive dolomitite, breunneritite, and sedimentary carbonates is shown in Fig. 9c. It is clear that the intrusive dolomitite pattern differs from that of the breunneritite in containing more REE and Y but is depleted in Nb, Ta, Zr, and Hf. The intrusive dolomitite is richer than the breunneritite in most trace elements, but is relatively depleted in Nb, Ta, Zr, and Hf. The breunneritite pattern is more similar to that of sedimentary carbonates, except for relative enrichment in LREE.

Albitite

Representative chemical analyses as well as normative compositions of Wadi Tarr albitites are given in Table 5. In terms of major element compositions, the Tarr albitites are comparable with typical albitites discussed by Kinnaird and Bowden (1991). Chemically, albitites are similar to oceanic plagiogranites, but this name is not suitable as the Tarr albitites are not associated with any ophiolite. The albitite is broadly granitic, as SiO₂ contents range from 67.2 to 69.6 wt%. This is also reflected by the differentiation index (DI = Q + Or + Ab + Lc + Ne + Kp) between 91.7 and 97.4%. Most of the normative salic minerals are albitite (78.7–91.3%), reflecting the high contents of Al₂O₃ (17–19 wt%)

Table 5 Chemical analyses and normative compositions of the albitites

Oxides	Subvolcanic albitite							Volcanic albitite			Averages of ED albititic rocks	
	T ₁	T ₉	T ₁₁	T ₁₇	S ₆ *	T ₁₉ *	T ₂₆ *	S ₂ *	S ₄ *	G ₆	1	2
SiO ₂	68.05	67.72	68.07	68.18	68.96	69.35	69.13	69.47	69.63	67.19	68.77	75.28
TiO ₂	0.37	0.40	0.69	0.55	0.36	0.30	0.29	0.33	0.31	0.55	0.01	0.04
Al ₂ O ₃	17.23	18.00	18.57	18.43	18.87	18.70	18.69	18.60	18.78	19.01	18.26	13.34
Fe ₂ O ₃	0.42	0.30	0.41	0.36	0.34	0.36	0.33	0.35	0.28	0.44	0.31	0.75
MnO	0.01	0.01	0.01	0.01	0.01	0.01	0.01	0.01	0.01	0.01	0.09	0.16
MgO	0.11	0.06	0.42	0.27	0.00	0.00	0.00	0.00	0.00	0.31	0.02	0.05
CaO	0.55	0.51	0.51	0.51	0.49	0.49	0.59	0.38	0.25	0.40	0.07	0.27
Na ₂ O	11.25	10.79	9.30	10.20	10.38	10.48	10.55	10.49	10.61	10.29	10.06	5.42
K ₂ O	0.12	0.12	0.15	0.14	0.31	0.12	0.15	0.24	0.13	0.16	0.14	3.54
P ₂ O ₅	0.23	0.18	0.15	0.16	0.28	0.19	0.27	0.12	0.00	0.14	<0.01	0.02
LOI	0.87	1.01	0.89	0.61	–	–	–	–	–	0.82	0.46	0.64
Total	99.18	99.11	99.19	99.42	100.00	100.00	100.01	99.99	100.00	99.31	98.19	99.51
CIA	46.74	48.88	53.09	50.77	50.76	50.59	50.12	50.53	50.99	51.60	52.04	50.17
Trace elements in ppm												
Ba	76	79	102	97	59	29	27	18	33	63	18	22
Rb	20>	20>	20>	21	7.9	2.2	3.4	5.0	2.7	20>	114	573
Sr	131	141	213	180	82	118	78	67	79	135	11	11
Y	12	13	14	15	26.0	34.7	31.3	2.9	2.7	9	42	171
Nb	26	16	13	21	21	21.9	18.4	7.5	8.4	10>	31	206
Zr	274	229	211	222	334	277	264	170	161	140	57	203
Ni	10	26	77	55	4	3	3	2	4	14	–	–
V	19	17	88	62	22	20	18	15	16	43	–	–
Cr	8	30	90	61	2	1	5	8	19	20	–	–
Pb	–	–	–	–	1.7	3.9	4.3	1.2	0.1	–	48	157
Ga	–	–	–	–	24.9	22.8	24.9	24.8	27.6	–	44	39
Th	–	–	–	–	7.2	3.8	6.3	7.5	6.5	–	22	65
Normative compositions												
Quartz	5.60	4.05	12.11	7.27	7.14	7.42	6.69	7.06	6.89	5.80		
Corundum	0.00	0.00	2.54	0.96	1.24	0.90	0.75	0.68	0.73	1.52		
Orthoclase	0.71	0.71	0.89	0.83	1.83	0.71	0.89	1.42	0.77	0.95		
Albite	87.97	91.29	78.69	86.30	87.82	88.67	89.26	88.75	89.77	87.66		
Anorthite	0.00	0.34	1.55	1.48	0.60	1.19	0.00	1.10	1.24	1.07		
Acmite	0.67	0.00	0.00	0.00	0.00	0.00	0.00	0.00	0.00	0.00		
NaMetasilica	1.50	0.00	0.00	0.00	0.00	0.00	0.00	0.00	0.00	0.00		
Diopside	0.46	0.10	0.00	0.00	0.00	0.00	0.00	0.00	0.00	0.00		
Wollastonite	0.00	0.00	0.00	0.00	0.00	0.00	0.00	0.00	0.00	0.00		
Hypersthene	0.06	0.10	1.05	0.67	0.00	0.00	0.00	0.00	0.00	0.77		
Magnetite	0.00	0.00	0.00	0.00	0.00	0.00	0.00	0.00	0.00	0.00		
Hematite	0.00	0.16	0.21	0.19	0.19	0.20	0.18	0.19	0.16	0.27		
Ilmenite	0.36	0.27	0.40	0.34	0.32	0.34	0.30	0.32	0.25	0.46		
Sphene	0.44	0.63	0.00	0.00	0.00	0.00	0.00	0.00	0.00	0.00		
Rutile	0.00	0.00	0.48	0.37	0.19	0.12	0.13	0.16	0.18	0.32		
Apatite	0.54	0.43	0.36	0.38	0.66	0.45	0.64	0.28	0.00	0.38		
D.I.	94.28	96.05	91.69	94.40	96.79	96.80	96.84	97.23	97.43	94.41		

*Indicates samples analyzed at Shimane U., others analyzed at Saudi Geological Survey, Jeddah, Saudi Arabia

1 average of Um Ara albitite, Eastern Desert of Egypt (Abdalla et al. 1996)

2 average of albitized microgranite of Um Ara, Eastern Desert of Egypt (Abdalla et al. 1996)

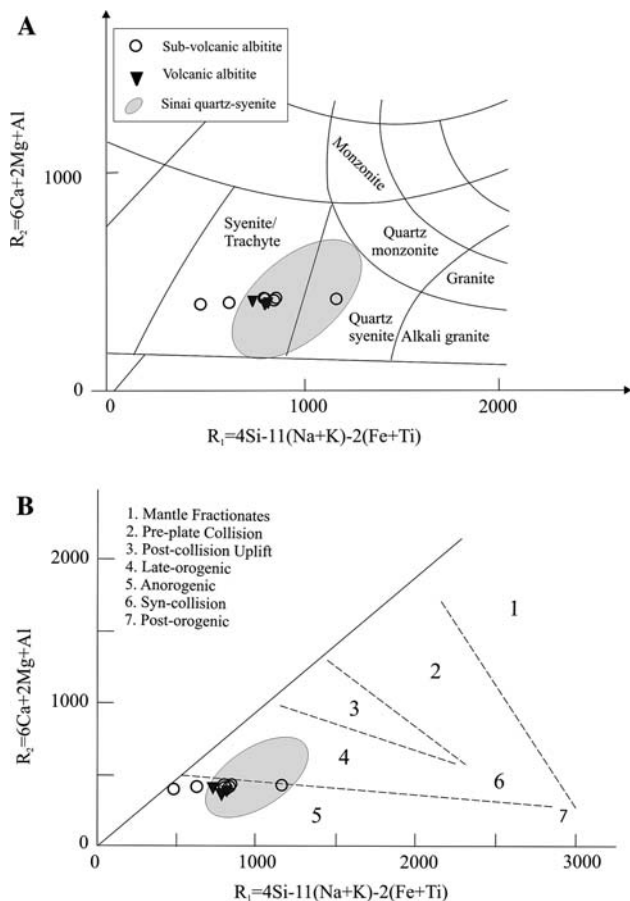


Fig. 10 **a** Classification of Wadi Tarr albitites using R_1 – R_2 diagram (De la Roche et al. 1980). **b** Plots of albitites on R_1 – R_2 diagram (De la Roche et al. 1980). Fields of tectonic setting based on Batchelor and Bowden (1985). The data of Sinai quartz–syenites are adopted from El-Tokhi (2001) and Azer (2006)

and Na_2O (9.3–11.3 wt%). The broadly granitic composition of the albitite is also seen in its low Ti, Mg, Fe, and P contents. Extreme enrichment in Na_2O is accompanied by remarkably low K_2O contents (0.12–0.31%). Low K_2O contents of the albitite may be due to nearly complete loss of magmatic potassium, as demonstrated by fenitization of wall rocks (Fig. 4h). Such extreme fractionation of alkalis is typical of high temperature hydrothermal systems associated with porphyry copper deposits (Lowell and Guilbert 1970).

On R_1 – R_2 classification diagram (De la Roche et al. 1980), Wadi Tarr albitites plot mainly in the syenite/trachyte field (Fig. 10a), except for one sample in the quartz–syenite field. The albitites show broad similarity to A-type granitic rocks of southern Sinai. This is further supported by the R_1 – R_2 multication parameters (De la Roche et al. 1980) in the diagram of Batchelor and Bowden (1985) where the albitites fall in the field of anorogenic granitoids (Fig. 10b). The presence of normative acmite in sample T_1 indicates the peralkaline nature of the albitite.

Compared to typical granitic rocks, Tarr albitites contain low abundances of most trace elements, especially compared to southern Sinai alkali syenites (El-Tokhi 2001; Azer 2006) and Israel (Mushkin et al. 2003). The eastern, porphyritic albitites have lower abundances of Y, Nb, and Zr than the western, equigranular albitites. REE abundances for Tarr albitites are reported for the first time here (Table 6, Fig. 11a). Chondrite-normalized REE plots show significant differences in both abundances and patterns. The subvolcanic albitite has a wide range of REE contents ($\sum REE = 39.3$ – 134.8 ppm) as does as the volcanic albitite ($\sum REE = 10.0$ – 84.6 ppm). It shows light REE enrichment (except sample T_{19} ; $[La/Lu]_n = 1.0$ – 7.4) and flat heavy REE profiles ($[Gd/Lu]_n = 0.80$ – 1.34), typical for ~ 600 Ma ANS granitic rocks. REE depletion in samples T_{19} and S_2 can be attributed to the absence of LREE-rich accessory phases such as monazite. Compared with the syenitic rocks of southern Sinai (Azer 2006) and Israel (Mushkin et al. 2003), the Tarr albitites have lower REE contents (Fig. 11a).

Slightly negative Eu-anomalies ($Eu/Eu^* = 0.67$ – 0.82) in the subvolcanic albitites is similar to ~ 600 Ma A-type ANS granites and may indicate early fractionation of plagioclase, perhaps in association with a strongly reduced melt (Hanson 1978; McKay 1989). Volcanic albitites (samples S_2 and S_4) show a remarkably wide range of LREE enrichment $[La/Lu]_n = (1.3$ – $28.2)$, but are like ~ 600 Ma A-type ANS granitic rocks in showing approximately flat heavy REE ($[Gd/Lu]_n = 0.88$ – 1.34). Volcanic albitite sample S_4 has light REE contents that overlap those of the subvolcanic albitites (samples S_6 and T_{26}). Volcanic albitite sample S_2 shows positive Eu-anomaly which may be due to the accumulation of feldspar. Fractionation of LREE and HREE largely depend on the nature of the crystallizing accessory phases, where zircon will deplete the melt in HREE, apatite in MREE and monazite in LREE (Rollinson 1994). The large range of observed REE fractionation and other evidence for unusual fractionations in the albitites are difficult to explain with simple crystal–liquid equilibrium (such as K/Na) suggests that vapor-phase fractionations were responsible.

A MORB-normalized multi-element diagram for average volcanic and sub-volcanic Tarr albitites is shown in Fig. 11b. The albitites show similar patterns of LILE enrichment. The volcanic albitite is more depleted in the HFSE and REE than the subvolcanic albitite, perhaps due to a greater role of accessory minerals or vapor phase.

Isotopic results

The albitites have a restricted range of initial $^{87}Sr/^{86}Sr$ (0.7035–0.7038; Table 7) and $\epsilon Nd_{605 Ma}$ (+4.3 to +6.4; Table 8). These are similar to the isotopic composition of other ~ 600 Ma igneous rocks from the region (Beyth et al.

Table 6 REE and some trace elements by ICP-MS in the albitites

Element	Sub-volcanic albitite			Volcanic albitite	
	S6	T19	T26	S2	S4
La	26.93	4.47	27.61	0.90	25.12
Ce	46.75	7.58	47.49	2.53	31.87
Pr	6.92	1.41	7.12	0.57	4.17
Nd	28.44	7.05	29.76	2.98	18.08
Sm	5.15	1.94	5.08	0.58	2.19
Eu	1.02	0.67	1.00	0.45	0.37
Gd	4.22	3.17	4.06	0.54	1.04
Tb	0.57	0.60	0.65	0.07	0.11
Dy	3.65	4.34	4.61	0.46	0.55
Ho	0.72	1.01	0.97	0.10	0.10
Er	2.15	2.94	2.78	0.30	0.32
Tm	0.34	0.47	0.44	0.05	0.06
Yb	2.28	3.15	2.81	0.42	0.53
Lu	0.39	0.49	0.43	0.08	0.10
∑REE	129.53	39.29	134.81	10.02	84.61
(Eu/Eu*) _n	0.67	0.82	0.67	2.45	0.75
(La/Lu) _n	7.41	0.98	6.93	1.28	28.17
(La/Sm) _n	3.38	1.49	3.51	1.01	7.39
(Gd/Lu) _n	1.34	0.80	1.18	0.88	1.34
Li	0.220	0.181	0.496	0.273	0.291
Be	1.446	2.378	1.779	2.050	1.171
Rb	4.985	0.680	1.895	3.677	0.538
Zr	334.240	277.483	264.165	170.234	160.857
Y	20.588	32.825	29.346	2.851	3.069
Nb	18.992	20.228	18.957	6.322	7.523
Sb	0.235	0.123	0.246	0.461	0.314
Cs	0.121	0.155	0.145	0.094	0.043
Ba	58.381	39.377	20.673	16.987	39.095
Hf	8.009	7.405	6.135	3.939	4.123
Ta	1.295	1.177	1.476	0.512	0.485
Pb	1.590	2.590	3.278	1.263	1.080
Th	5.109	2.957	4.614	7.598	5.525
U	0.970	0.563	0.985	1.057	0.903

1994; Katzir et al. 2007). Nd model ages (T_{DM} , method of DePaolo 1988) are 0.64–0.79 Ga, at the low end of the range observed for other igneous rocks from Sinai and Jordan (Stern 2002), but still consistent with an interpretation that these were Late Neoproterozoic juvenile melts. Isotopic compositions of the associated intrusive carbonates are variable, with the dolomitite initial isotopic composition ($^{87}\text{Sr}/^{86}\text{Sr} = 0.70356$, $\epsilon\text{Nd}_{605\text{ Ma}} = +5.49$, $T_{DM} = 0.71$ Ga) being very similar to that of the albitite, while the breunneritite has a much more radiogenic initial $^{87}\text{Sr}/^{86}\text{Sr}$ (0.70896), although ϵNd is slightly lower than that of the dolomitite and albitites (+3.77); no Nd model age is calculated because of high $^{147}\text{Sm}/^{144}\text{Nd}$. Initial Sr

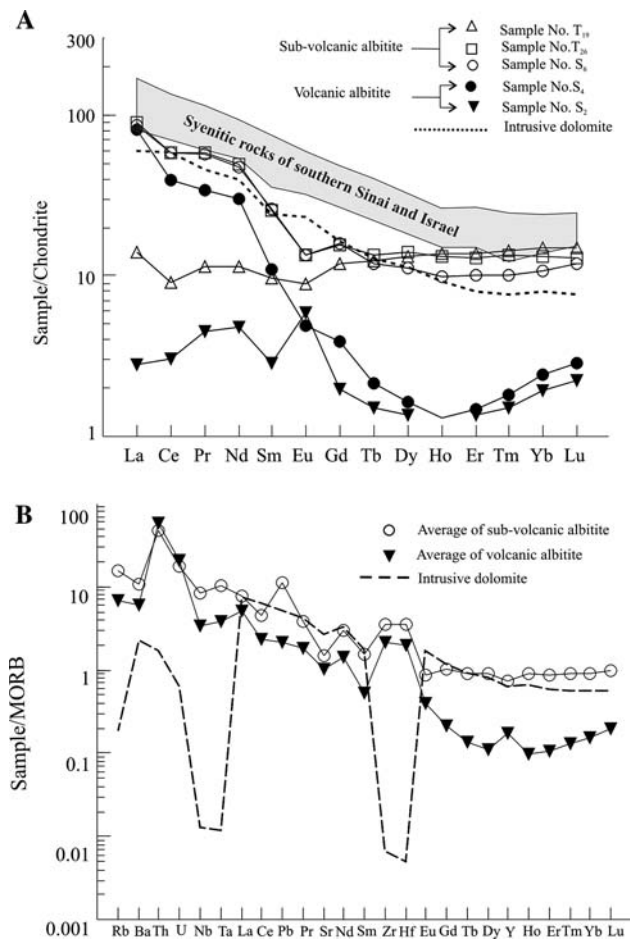


Fig. 11 **a** Chondrite-normalized REE patterns for the albitites (using the chondrite values of Boynton 1984); Quartz–syenite of Sinai adopted from Azer (2006); those of southern Israel are after Mushkin et al. (2003). **b** MORB-normalized spider diagram for the albitites. Normalization values are taken from Pearce and Parkinson (1993)

and Nd isotopic compositions are shown on Fig. 12 along with data from Bogoch et al. (1986). Our results confirm the large differences that Bogoch et al. (1986) found for especially Sr isotopic compositions of the dolomitite and breunneritite. The breunneritite $^{87}\text{Sr}/^{86}\text{Sr}$ seems to be in equilibrium with that of ~600 Ma seawater (Halverson et al. 2007). Our results also show the similarity in isotopic composition between the albitite and the intrusive dolomitite, supporting the interpretation that these are petrogenetically linked. Isotopic compositions of two sedimentary carbonates are very similar, with initial $^{87}\text{Sr}/^{86}\text{Sr}$ similar to what would be expected for 850 Ma seawater (Halverson et al. 2007). The sedimentary carbonates have much lower initial $^{87}\text{Sr}/^{86}\text{Sr}$ than the breunneritite. The combined Sr–Nd isotopic compositions of the sedimentary carbonates also fall outside the large field defined by the intrusive dolomitite.

Table 7 Rb–Sr concentrations and Rb–Sr isotopic data

Sample	Rb (ppm)	Sr (ppm)	$^{87}\text{Rb}/^{86}\text{Sr}$	$^{87}\text{Sr}/^{86}\text{Sr}$	$(^{87}\text{Sr}/^{86}\text{Sr})_i^*$
S2	3.66	67.4	0.1579	0.704892 ± 16	0.70353
S4	0.54	79.2	0.0198	0.703703 ± 15	0.70370
S6	4.99	82.2	0.1759	0.705274 ± 16	0.70376
100	0.24	237.5	0.0029	0.703589 ± 14	0.70356
200	0.77	108.8	0.0205	0.709137 ± 16	0.70896
28A	0.80	136.0	0.017	0.705454 ± 16	0.70531
28B	0.30	112.4	0.0077	0.705411 ± 16	0.70535

NIST SRM987 Sr standard $^{87}\text{Sr}/^{86}\text{Sr} = 0.710244$

*Corrected for 605 Ma of radiogenic growth

Petrogenesis

Intrusive carbonates

The petrogenesis of carbonatites remains a matter of debate (Gittins and Harmer 2003; Woolley 2003). Isotopic and trace element data are needed to distinguish between mantle-derived carbonate and sedimentary carbonates that have somehow been remobilized (Barker 1993). Most carbonatites suggest a mantle origin by being intimately related to alkaline mafic igneous rocks. However, Lentz (1999) concluded that carbonatites may be not exclusively derived from mantle melts. Late stage hydrothermal, metasomatic, and metamorphic carbonatites are also reported (Höy and Kwong 1986; Pell and Höy 1989; Scogings and Forster 1989; Le Bas et al. 2002; Srivastava et al. 2005b). Bogoch et al. (1986) interpreted the Tarr dolomitite to have formed in equilibrium with melting of depleted mantle. This carbonate-bearing peridotite was emplaced higher in the crust as a result of regional shearing and extension. The carbonate was extracted as a result of metamorphism and was emplaced at its present position as “hydrothermal-type” vein and replacement deposits. Hydrothermal activity continued after emplacement, and portions of the dolomitite were converted by this activity to breunnerite. Other authors (Shimron

1975; Blasy et al. 2001) relate the origin of the intrusive carbonates of Wadi Tarr to the albitites.

In Wadi Tarr, the host rocks of the intrusive carbonate–albitite complex are metamorphosed to greenschist facies, but nearby reach amphibolite facies (Reymer 1983). In general deformation and metamorphism around the carbonate sediments was accompanied by the migration of carbonate-rich solutions, as shown by veins and dikes of calcite and dolomite, less typically ankerite, magnesite, and breunnerite. Experimental studies indicate that carbonate magmas could be produced by melting sedimentary carbonates (Wyllie and Tuttle 1960; Fanelli et al. 1986). The presence of Neoproterozoic sedimentary carbonates (marbles) near the intrusive carbonate–albitite complex suggests the possibility that these were remobilized to generate the intrusive carbonates; however, the quantity appears to be insufficient and furthermore these are folded into an open synform and unlikely to have reached the depths necessary for anatexis (Shimron 1975).

Carbonate melts can also form when hydrothermal fluids interact with ultramafic rocks, especially serpentinites (Deer et al. 1992). However serpentinites are uncommon in Sinai (Beyth et al. 1978). Serpentine, a few tens of meters in length, intrude (Madbouly 1991; Moussa 2002) or are tectonically emplaced (Abu El-Enen and Makroum 2003) migmatites and gneisses at Kabr El-Bonaya in south Sinai. Considering these criteria, we exclude the formation of the intrusive dolomitite as remobilized sedimentary or serpentinite-derived carbonates as a result of metamorphism or due to the intrusion of albitite.

Isotopic data for Tarr dolomitite (mean $\delta^{18}\text{O} = +6.9$; mean $\delta^{13}\text{C} = -8.1$; mean $\epsilon_{\text{Nd}} = +3.4$; $^{87}\text{Sr}/^{86}\text{Sr} = 0.70342\text{--}0.70562$; Bogoch et al. 1986; this study) suggests that the dolomitite is derived from a mantle or juvenile crustal or magmatic source, while the isotopic composition of the breunnerite (mean $\delta^{18}\text{O} = +18.85$; mean $\delta^{13}\text{C} = -6.1$; mean $\epsilon_{\text{Nd}} = +2.2$; mean $^{87}\text{Sr}/^{86}\text{Sr} = 0.70805$; Bogoch et al. 1986; this study) was at least partly re-equilibrated with seawater or sedimentary carbonate sources. This

Table 8 Sm–Nd concentrations and Sm–Nd isotopic data

Sample	Sm (ppm)	Nd (ppm)	$^{147}\text{Sm}/^{144}\text{Nd}$	$^{143}\text{Nd}/^{144}\text{Nd}$	$\epsilon_{\text{Nd}(605)}$	T_{DM} (Ga)
S2	0.58	2.98	0.1177	0.512658 ± 11	+6.37	0.64
S4	2.19	18.08	0.0732	0.512452 ± 11	+5.79	0.66
S6	5.15	28.44	0.1095	0.512517 ± 10	+4.25	0.79
100	4.69	23.99	0.1182	0.512615 ± 10	+5.49	0.71
200	0.45	1.16	0.2345	0.512988 ± 10	+3.77	–
28A	0.58	2.72	0.1287	0.512592 ± 10	+4.33	–
28B	0.45	2.05	0.13334	0.512596 ± 10	+4.03	–

ϵ_{Nd} calculated at 605 Ma ago

La Jolla standard $^{143}\text{Nd}/^{144}\text{Nd} = 0.511866$

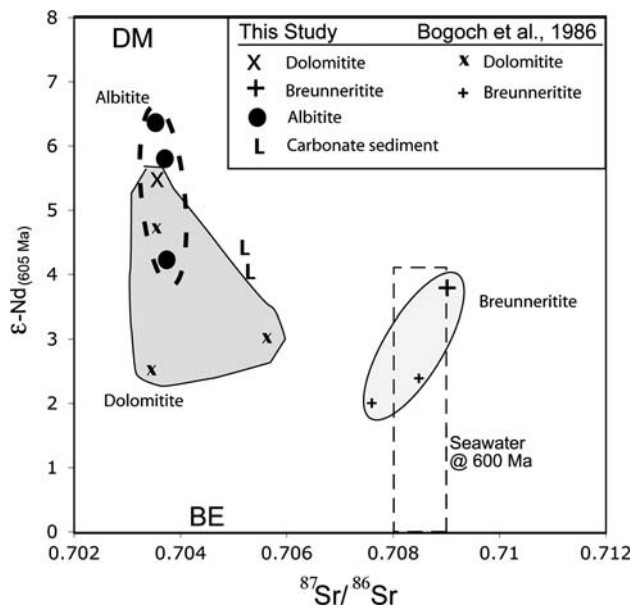


Fig. 12 Initial isotopic compositions of Sr and Nd for albitite, dolomitite, breunneritite, and sedimentary carbonates from this study and for intrusive carbonates from Bogoch et al. (1986). Approximate position of 600 Ma old depleted mantle (DM; from DePaolo 1988; $^{87}\text{Sr}/^{86}\text{Sr}$ estimated based on linear evolution from 0.6998 for initial bulk Earth to ~ 0.7035 today), bulk Earth (BE; $\epsilon_{\text{Nd}} = 0$; $^{87}\text{Sr}/^{86}\text{Sr}$ estimated from linear growth of Bulk Earth 0.6998 for initial bulk Earth to ~ 0.7050 today) and seawater (dashed box, approximate range for Sr isotopes only from Halverson et al. 2007) are shown for comparison

re-equilibration probably occurred when the dolomite was replaced by breunnerite.

The association of albitite and breccia at Tarr is reminiscent of associations found for magmatic cupolas in some porphyry copper and gold deposits, but for a volatile-carbonate A-type magma instead of a hydrous calc-alkaline magma. The term cupola refers to any domical region at the upper boundary between crystallized pluton and the remaining body of magma (Cloos 2001). The difference between well-documented cupolas and Tarr may relate to the very different nature of volatiles in the magmas, with porphyry copper being water-rich and Tarr albitite being CO_2 rich. The presence of CO_2 in Tarr cupola can induce immiscibility both within the magmatic volatile phase and in hydrothermal systems. Field and geochemical evidences for immiscibility between carbonate and silicate magmas have been presented by many authors (e.g. Taubald et al. 2004; Halama et al. 2005). Liquid immiscibility led to exsolution of a carbonate fluid from a silicate melt, probably an A-type granite pluton. Viscosity differences segregated the magma into a fraction comprising silicate magma with scatter carbonate globules and fraction comprising carbonates (Macdonald et al. 1993). A liquid immiscibility relationship between the silicate magma and carbonate is indicated by the presence of spherical patches of carbonate in diabase dykes

which intrude the Tarr albitite complex (Bogoch and Magaritz 1983). Dolomite is the main component of carbonate patches, which are geochemically and isotopically similar to the intrusive dolomitite.

Our study shows that the intrusive carbonates were closely related to explosive emplacement of the albitite, and that explosive brecciation was due to volatile overpressure. A simple explanation for these relations is that the conversion of CO_2 from supercritical fluid to gas at low pressures was responsible. CO_2 exsolving from a subjacent magma body would have risen as a supercritical fluid into the cupola region, where it changed into gas at $P < \sim 70$ atm (a few hundred meters depth, assuming lithostatic pressures). The conversion of CO_2 fluid into gas results in a volume expansion of $\sim 850\times$, which must have been explosive, causing the brecciation. The carbonate liquid separated from silicate magma crystallized into dolomite, cementing the breccia. Dolomitite–albitite formation in this cupola was accompanied or followed by development of a robust hydrothermal system, further indicating that this was a hypabyssal system.

Albitite

Albitites are unusual rocks and several petrogenetic models have been proposed for them globally. Their origin is ascribed to the action of metasomatic-hydrothermal fluids on granitoids (Demange 1975; Kovalenko 1978; Chauris 1985; Cathelineau 1988; Rugless and Pirajno 1996) or they are a variant of A-type magma (Schwartz 1992; Chaudhri et al. 2003). Similar controversies surround the origins of “massif-type anorthosites”. Albitites with compositions similar to Tarr albitites are reported from Um Ara area in the Eastern Desert of Egypt (Abdalla et al. 1996; see the averages of Um Ara albitite in Table 5). These rocks, termed apogranite, are transitional between albitite and A-type granites, as their albitite content is generally less than 50% and quartz, microcline and mica are common (Helba et al. 1997). Moreover, they are enriched in Nb, Y, Rb, Ta and Ga relative to Tarr albitites. Apogranite occurs as a marginal phase of normal, frequently subalkaline granites and grade into them via a zone of albitized granite. There is also a controversy regarding whether Egyptian apogranites formed from normal granites by post-magmatic high-temperature metasomatism (Sabet et al. 1976a, b; El-Tabal 1979; Riad 1979) or by igneous processes followed by modest post/late magmatic alteration (Helba 1994; Helba et al. 1997; Arslan et al. 1997; Abou El Maaty and Ali Bik 2000). The Sinai albitites are not obviously connected with a granite pluton, although they are situated in the midst of a volcano–plutonic complex that may be a caldera complex (Fig. 2). This interpretation is supported by similar ages (604–608 Ma) for nearby alkaline granitic rocks (Fig. 1; Be’eri-Shlevin et al. 2008b in press, Be’eri-Shlevin 2008a).

Interpretations of Tarr albitite genesis are also diverse. Shimron (1975) considered that they formed as a result of fractional crystallization and liquid immiscibility acting on a highly gas-charged, slow-cooling gabbroic magma, ultimately derived from an upper mantle source. Bogoch et al. (1987) argued that the Tarr albitite formed by Na-metasomatism, based on high $\text{Na}_2\text{O}/\text{K}_2\text{O}$ and occurrence of gradational contacts and ghost structures through albitite rocks. Soliman et al. (1992) considered that the parent magma of the Wadi Tarr albitite was alkali-syenite, but noted that immobile incompatible trace element abundances are much lower than expected for alkali syenites in the area. Blasy et al. (2001) concluded that the albitites are alkaline, with affinities to highly fractionated A-type granites. They modified Shimron's (1975) model and suggested that fractional crystallization and liquid immiscibility of an alkaline gabbro resulted in alkali mafic magma (basaltic dykes), intrusive carbonate, and albitites.

Several observations are pertinent for deciding whether the albitites of Wadi Tarr are mostly magmatic or metasomatic in origin. The albitites are composed of primary albite, have undergone little post-crystallization alteration and there is no indication of Na-metasomatism. The chemical index of alteration ($\text{CIA} = \text{molecular } [\text{Al}_2\text{O}_3 / (\text{Al}_2\text{O}_3 + \text{CaO} + \text{Na}_2\text{O} + \text{K}_2\text{O})] \times 100$) in the albitites varies between 46.7 and 53.1 (Table 5), within the range of fresh granites (45–55; Nesbitt and Young 1982). The isotopic compositions of Sr and Nd lie within the range of normal magmatic rocks in the region. Initial Sr and Nd isotopic compositions for ~600 Ma granitic rocks in the vicinity of the Tarr Complex are ~0.7040 and +5, respectively (Y. Katzir personal communication 2008), and the isotopic compositions of the albitites (Fig. 12) are very similar to these clearly magmatic rocks of similar age. From these considerations, we agree with Shimron (1975) that the Tarr albitites are mostly magmatic products.

There are nevertheless many questions about how albitite magma could form. From liquidus–solidus relationships in the haplogranitic system Ab–Or–H₂O (Holtz et al. 1992), it is clear that albitite cannot form by crystal fractionation of granitic magma alone. However, the albitite may represent residual magma remaining after near-total crystallization of an A-type granite pluton that was affected by unusual fluid-related processes, forcibly emplaced into the roof above the cooling pluton. The hypersolvus nature of the Tarr albitite is consistent with shallow emplacement and a high temperature of crystallization similar to that of other alkaline rocks emplaced at relatively shallow depth (Tuttle and Bowen 1958; Martin and Bonin 1976; Lowenstern et al. 1997). The relatively high temperature coupled with the fluxing effect of the volatiles promoted fluidity that may have enabled the albititic magma to rise to high levels in the crust, ultimately reaching the top of the pluton and locally erupting as lava

flows. The CO₂-rich nature of the evolving magmatic fluid may have led to unusual and poorly understood liquid lines of descent to yield the albitite residual liquid. We suspect that the parent magma of the albitite was alkali granite. The early fractional crystallization of feldspar and mafic minerals deeper in a crustal magma chamber may have enriched Na, Si and volatiles in the residual melt which naturally migrated to the top of the magma body. Further understanding of how the Tarr albitite formed will require more study.

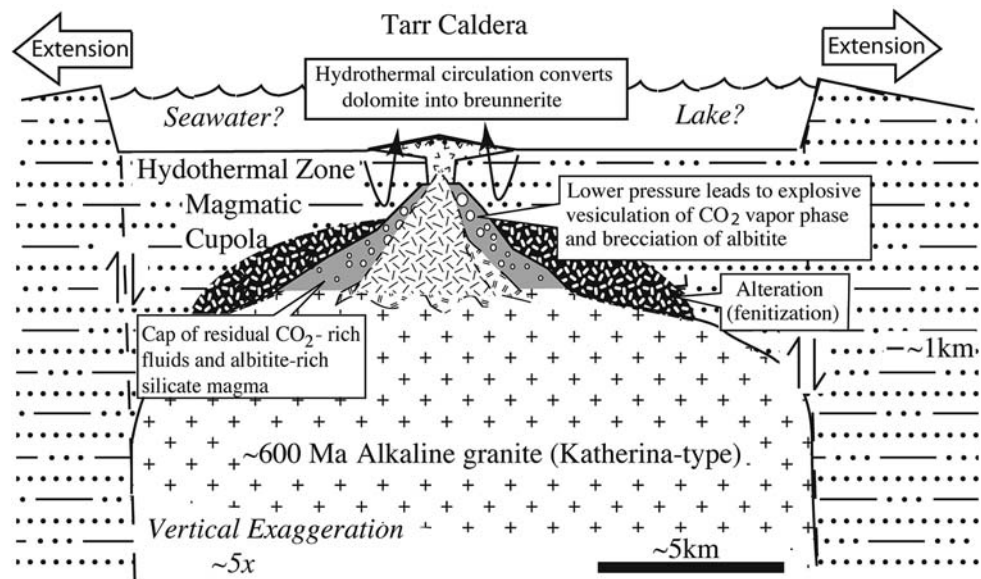
There are two indications of strong high-temperature hydrothermal and magmato-thermal alteration around the Tarr complex, both related to the emplacement of albitite and intrusive carbonates. Hydrothermal activity is reflected in the formation of breunnerite, which required large water:rock ratios in order to effect the large changes in Sr and O isotopic compositions observed, and for which equilibration with seawater is indicated. Magmatothermal alteration is also indicated by the amphibolitized and fenitized aureole of country rocks. Fenitization includes intense sodium and potassium metasomatism whereby rocks are replaced by albite, phlogopite, and K-feldspar; in the case of Tarr, the potassium was derived from late magmatic fluids expelled from the intrusion. Shimron (1975) noted that fenitization was most conspicuous around the intrusion breccias and extends a few hundred meters beyond this; tourmaline veins occur 2 km east of the Tarr albitite.

We infer that Tarr albitite, intrusion breccia, intrusive carbonates, and hydrothermal system express a magmatic cupola above an A-type granite pluton. This hypabyssal magmatic system may have been part of a large volcanic caldera (Fig. 13), although further studies are needed to determine whether or not the volcanic and volcanoclastic rocks surrounding Tarr define a caldera complex of the correct age and composition. Under extension, residual magma and volatiles concentrated in the cupola, explosively degassing around residual albitite magma. Wall-rock alteration or fenitization occurred around the intrusive complex. Fenitization and dolomitite are the products of magmatic volatiles, breunneritization reflects hydrothermal alteration of the dolomitite by Ediacaran seawater (Fig. 13), probably shortly after dolomitite emplacement, while the magmatic system was still hot enough to power formation of a hydrothermal cell.

Summary

Tarr complex comprises hypabyssal and volcanic albitite masses surrounding by an emplacement breccia containing veins and dykes of carbonates. Cross-cutting relationships and other field relationships indicate that the carbonate–albitite complex is an intrusive complex that is younger than the surrounding Precambrian rocks. The albitites and

Fig. 13 Cartoon section of Tarr magmatic cupola, modified after Cloos (2001). Tarr intrusive carbonate–albitite complex represents residual magma emplaced at shallow levels above a Katherina-type A-type granite pluton (Katzir et al. 2007)



Wadi Kid core complex (Blasband et al. 2000) are aligned similarly, suggesting similar responses to regional extension, perhaps related to movements on the left-lateral Najd shear system or due to orogenic collapse. Zircons separated from the albitites yield a U–Pb age of 605 ± 15 Ma and this is also the age of the intrusive carbonates. Geochemical signatures of Tarr albitites indicate that they represent pristine igneous rocks and are not metasomatic products. Tarr albitites are relatively more fractionated, alkaline and related to ANS A-type magmas. Isotopic data of the albitite and intrusive dolomitite of Wadi Tarr clearly indicate a mantle source, like that responsible for ANS A-type granites. The association of albitite and volcanic breccia is very reminiscent of associations found for magmatic cupolas associated with porphyry copper deposits. Therefore, Tarr albitite and explosion breccia may represent late magmatic activity in a cupola at hypabyssal depths above a ~600 Ma A-type granite.

The Tarr albitite and intrusive dolomitite represent a rare example of a liquid immiscibility of silicate magma and carbonate fluid. The breunnerite is a secondary replacement of dolomitite, with isotopic compositions indicating re-equilibration with seawater, probably marking the roots of a vigorous hydrothermal system.

Acknowledgments We appreciate stimulating discussions with Prof. M.D. Samuel of the Egypt National Research Centre. We greatly appreciate the assistance of K. Ali and M. Whitehouse for zircon dating, B. Woldemichael for isotopic analyses and Y. Sawada for XRF facility. We thank Yaron Be’eri-Shlevin for sharing new geochronologic results on Sinai granites and the use of Fig. 1. This research was partly supported by NSF OCE 0804749 under the US–Egypt Joint Fund Program. The NordSIM ion microprobe facility is financed and operated under an agreement between the research councils of Denmark, Norway, Sweden, and the Geological Survey of

Finland and the Swedish Museum of Natural History; this is NordSIM publication number 222.

References

- Abdalla HM, Ishihara S, Matsueda H, Abdel Monem AA (1996) On the albitite-enriched granitoids Um Ara area, Southeastern Desert, Egypt. 1. Geochemical, ore potentiality and fluid inclusion studies. *J Geochem Explor* 57:127–138. doi:10.1016/S0375-6742(96)00029-5
- Abou El Maaty MA, Ali Bik MW (2000) Petrology of alkali feldspar granites of Nuweibi and Gebel El-Mueilha, central Eastern Desert, Egypt. *Egypt J Geol* 44:127–148
- Abu El-Enen MM, Makroum FM (2003) Tectonometamorphic evolution of the northeastern Kid Belt, Southeast Sinai, Egypt. *Ann Geol Surv Egypt* VXXVI:19–37
- Andresen A, El-Rus MAA, Myre PI, Boghdady GY (2008) Corfu F U–Pb TIMS age constraints on the evolution of the Neoproterozoic Meatiq Gneiss Dome, Eastern Desert, Egypt. *Int J Earth Sci* (in press)
- Arslan AI, Helba HA, Khalil SO, Morteani G (1997) Bedrock geochemical prospecting and ore potentiality of the rare metal-bearing granite at Nuweibi area, Central Eastern Desert, Egypt. In: 3rd inter geoch Alexandria univ proc, pp 375–387
- Azer MK (2006) The Petrogenesis of late Precambrian felsic alkaline magmatism in South Sinai, Egypt. *Act Geol Polon* 56:463–484
- Barker DS (1993) Diagnostic magmatic features in carbonatites: implication for the origins of dolomite- and ankerite-rich carbonatites. *S Afr J Geol* 96:131–138
- Batchelor RA, Bowden P (1985) Petrogenetic interpretation of granitoid rock series using multicationic parameters. *Chem Geol* 45:43–55. doi:10.1016/0009-2541(85)90034-8
- Be’eri-Shlevin Y (2008a) The origin and evolution of Neoproterozoic magmatism in the northern Arabian–Nubian-shield (Sinai Peninsula, Egypt and Southern Israel): evidence from the stable and radiogenic isotope record. PhD thesis, Ben-Gurion University
- Be’eri-Shlevin Y, Katzir Y, Whitehouse M (2008b) Post-collisional tectono-magmatic evolution in the northern Arabian–Nubian Shield (ANS): time constraints from ion-probe U–Pb dating of zircon. *J Geol Soc Lond* (in press)

- Bentor YK (1985) The crustal evolution of the Arabo–Nubian massif with special reference to the Sinai Peninsula. *Precam Res* 28:1–74. doi:[10.1016/0301-9268\(85\)90074-9](https://doi.org/10.1016/0301-9268(85)90074-9)
- Bentor YK, Eyal M (1987) The geology of Sinai, its implication for the evolution of the Arabo–Nubian massif, Jebel Sabbagh sheet. The Israel Academy of Sciences and Humanities, pp 484
- Beyth M, Grunhagen H, Zilberfarb A (1978) An ultramafic rock in the Precambrian of eastern Sinai. *Geol Mag* 115:373–378
- Beyth M, Stern RJ, Altherr R, Kröner A (1994) The Late Precambrian Timna igneous complex, Southern Israel: evidence for comagmatic-type Sanukitoid monzodiorite and alkali granite magma. *Lithos* 31:103–124. doi:[10.1016/0024-4937\(94\)90003-5](https://doi.org/10.1016/0024-4937(94)90003-5)
- Bielski M (1982) Stages in the evolution of the Arabian–Nubian massif in Sinai. PhD thesis, Hebrew University of Jerusalem, p 155
- Bielski M, Jager E, Steinitz G (1979) The geochronology of Iqna granite (Wadi Kid Pluton), Southern Sinai. *Contrib Miner Petrol* 70:159–165. doi:[10.1007/BF00374445](https://doi.org/10.1007/BF00374445)
- Blasband B, Brooijmans P, Dirks P, Visser W, White S (1997) A Pan-African core complex in the Sinai, Egypt. *Geol Mijnb* 76:247–266. doi:[10.1023/A:1003089218512](https://doi.org/10.1023/A:1003089218512)
- Blasband B, White S, Brooijmans P, De Boorder H, Visser W (2000) Late Proterozoic extensional collapse in the Arabian–Nubian Shield. *J Geol Soc Lond* 157:615–628
- Blasy M, Baroudy AF, Kharbish SM (2001) Geochemical characteristics of Wadi Tarr albitite, Southeastern Sinai, Egypt. *Egypt J Geol* 42:767–780
- Bogoch R, Magaritz M (1983) Immiscible silicate–carbonate liquids as evidenced from ocellar diabase dykes, Southeast Sinai. *Contrib Miner Petrol* 83:227–230. doi:[10.1007/BF00371190](https://doi.org/10.1007/BF00371190)
- Bogoch R, Halicz L, Nathan Y (1982) Breunnerite from the Tarr albitite complex, Sinai. *Am Miner* 67:822–825
- Bogoch R, Eldad H, Nathan Y (1984) Scandium-bearing carbonates of the Tarr albitite complex, Southeast Sinai. *Geochem Cosmochem Acta* 48:885–887. doi:[10.1016/0016-7037\(84\)90110-8](https://doi.org/10.1016/0016-7037(84)90110-8)
- Bogoch R, Magaritz M, Michard A (1986) Dolomite of possible mantle origin, Southeast Sinai. *Chem Geol* 56:281–288. doi:[10.1016/0009-2541\(86\)90009-4](https://doi.org/10.1016/0009-2541(86)90009-4)
- Bogoch R, Bahat D, Kisch H (1987) The Tarr albitite: a metasomatic plagiogranite from mainly non-intrusive protoliths. *Ophioliti* 12:8–22
- Boynton WV (1984) Cosmochemistry of the rare earth elements: meteorite studies. In: Henderson P (ed) *Rare earth element geochemistry*. Developments in geochemistry 2. Elsevier, Amsterdam, p 510
- Brassinnes S, Balaganskaya E, Demaiffe D (2005) Magmatic evolution of the differentiated ultramafic, alkaline and carbonate intrusion of Vuoriyarvi (Kola Peninsula, Russia), A LA-ICP-MS study of apatite. *Lithos* 85:76–92. doi:[10.1016/j.lithos.2005.03.017](https://doi.org/10.1016/j.lithos.2005.03.017)
- Brooijmans P, Blasband B, White SH, Visser WJ, Dirks P (2003) Geothermobarometric evidence for a metamorphic core complex in Sinai, Egypt. *Precam Res* 123:249–268. doi:[10.1016/S0301-9268\(03\)00071-8](https://doi.org/10.1016/S0301-9268(03)00071-8)
- Castorina F, Stoppa F, Cundari A, Barbieri M (2000) An enriched mantle source for Italy's melilitite–carbonatite association as inferred by its Nd–Sr isotope signature. *Miner Mag* 64:625–639. doi:[10.1180/002646100549652](https://doi.org/10.1180/002646100549652)
- Cathelineau M (1988) Accessory mineral alteration in peraluminous granites at the hydrothermal stage: a review. *Rend Soc Ital Miner Petrol* 43:499–508
- Chaudhri N, Kaur P, Okrusch M, Schimraszczyk A (2003) Characterization of the Dabla granitoids, North Khetri Copper Belt, Rayasthan, India: evidence of bimodal anorogenic felsic magmatism. *Gond Res* 6:879–895. doi:[10.1016/S1342-937X\(05\)71032-7](https://doi.org/10.1016/S1342-937X(05)71032-7)
- Chauris L (1985) Premières données géochimiques sur les albitites métasomatiques des environs de Brest (Finistère, France). *Bull Soc Geol Fr* 8:885–889
- Cloos M (2001) Bubbling magma chambers, cupolas, and porphyry copper deposits. *Int Geol Rev* 43:285–311
- De la Roche H, Leterrier J, Grandclaude P, Marchal M (1980) A classification of volcanic and plutonic rocks using R1–R2 diagrams and major-element analyses: its relation with current nomenclature. *Chem Geol* 29:183–210. doi:[10.1016/0009-2541\(80\)90020-0](https://doi.org/10.1016/0009-2541(80)90020-0)
- Deer WA, Howie RA, Zussman J (1992) An introduction to the rock forming minerals, 2nd edn. Longman Scientific and Technical, London, p 696
- Demange M (1975) Zonation métasomatique autour des albitites de la région de Saint Chély D' Apcher (Lozère). *Bull Soc Fr Miner Cristallogr* 98:186–190
- DePaolo DJ (1988) Neodymium isotope geochemistry. Springer, New York, p 187
- El-Gaby S, Khudeir AA, Abdel Tawab M, Attla RF (1991) The metamorphosed volcano-sedimentary succession of Wadi Kid, Southeastern Sinai, Egypt. *Ann Geol Surv Egypt* 17:19–35
- El-Haddad MA, Hashad MH (1984) The major and minor elements chemistry of Gebel Tarbtie carbonatites South, Egypt. *Bull Fac Sci Assuit Univ* 13:205–217
- El-Haddad MA, Gwozdz R, Heydorn K (1984) Carbonatites with peculiar trace element abundances. *Bull Fac Sci Assuit Univ* 13:191–203
- El-Metwally AA, El-Aasy IE, Ibrahim ME, Essawy MA, El-Mowafy AA (1999) Petrological, structural and geochemical studies on the basement rocks of Gabal Um-Zariq-Wadi Kid area, South Eastern Sinai. *Egypt J Geol* 43:147–180
- El-Nisr SA, Saleh GM (2001) Geochemistry and Petrogenesis of the Late Jurassic–Early Cretaceous Mansouri Ring Complex, Southeastern Desert, Egypt. *J Afr Earth Sc* 32:87–102. doi:[10.1016/S0899-5362\(01\)90020-X](https://doi.org/10.1016/S0899-5362(01)90020-X)
- El-Ramly MF, Budanov VI, Hussein AA (1971) The alkaline rocks of South Eastern Egypt. *Geol Surv Egypt*, 111 pp, paper No. 53
- El-Tabal HK (1979) Mineralogical studies on some rare metal apogranites from Nuweibi and Abu Dabbab areas, Eastern Desert, Egypt. MSc thesis, Al-Azhar Universiti, Cairo, pp 112
- El-Tokhi M (2001) Petrogenesis and geochemistry of some quartz-syenites from Southern Sinai, Egypt. 2nd inter conf geol afr Assiut Univ Egypt, pp 239–253
- Fanelli MT, Cava N, Wyllie PJ (1986) Calcite and dolomite without portlandite at a new eutectic in CaO–MgO–CO₂–H₂O with applications to carbonatites. In: *Morphology and phase of minerals*. Proceedings of the 13th general meeting of the International Mineralogical Association, Bulgarian Academy of Science, Sofia, 313–322
- Furnes H, Shimron AE, Roberts D (1985) Geochemistry of Pan-African volcanic arc sequences in Southeastern Sinai Peninsula and plate tectonic implications. *Precam Res* 29:359–382. doi:[10.1016/0301-9268\(85\)90043-9](https://doi.org/10.1016/0301-9268(85)90043-9)
- Gaby S, List FK, Tehrani R (1990) The basement complex of the Eastern Desert and Sinai. In: Said R (ed) *The geology of Egypt*. Balkema, Rotterdam, pp 175–184
- Gittins J (1989) The origin and evolution of carbonatite magmas. In: Bell K (ed) *Carbonatites: genesis and evolution*. Unwin Hyman, London, pp 580–600
- Gittins J, Harmer RE (2003) Myth and reality in the carbonatite-silicate rock “association”. *Period Miner* 72:19–26
- Hafez AMA, Abdel Wahed M, Shallaly NA (2007) Microfabric, geochemistry and clockwise P-T path of the Precambrian metasediments in the central Wadi Kid area, Southeastern Sinai. In: *The fifteen symposium on Precambrian and development (abstract)*

- Haidinger WM (1825) Treatise on Mineralogy. In: Mohs F (ed) translation with considerable additions. 3 volumes. Edinburg 1:411
- Halama R, Vennemann T, Siebel W, Markl G (2005) The Grønvedal-Ika carbonatite-syenite complex, South Greenland: carbonatite formation by liquid immiscibility. *J Petrol* 46:191–217. doi: [10.1093/petrology/egh069](https://doi.org/10.1093/petrology/egh069)
- Halverson GP, Dudás FO, Maloof AC, Bowring SA (2007) Evolution of the $^{87}\text{Sr}/^{86}\text{Sr}$ composition of Neoproterozoic seawater. *Palaeogeogr Palaeoclimatol Palaeoecol* 256:103–129. doi: [10.1016/j.palaeo.2007.02.028](https://doi.org/10.1016/j.palaeo.2007.02.028)
- Hanson GN (1978) The application of trace elements to the petrogenesis of igneous rocks of granitic composition. *Earth Planet Sci Lett* 38:26–43. doi: [10.1016/0012-821X\(78\)90124-3](https://doi.org/10.1016/0012-821X(78)90124-3)
- Harmer RE, Lee CA, Eglinton BM (1998) A deep mantle source for carbonatite magmatism: evidence from the nephelinites and carbonatites of the Buhera district, SE Zimbabwe, *Earth Planet. Sci Lett* 158:131–142. doi: [10.1016/S0012-821X\(98\)00053-3](https://doi.org/10.1016/S0012-821X(98)00053-3)
- Hashad MH (1981) Contributions to the mineralogy and geology of carbonate rocks within the basement complex of Egypt. Unpublished PhD thesis, Al-Azhar University, p 240
- Hashad AH, El-Reedy MWM (1980) Geochronology of the nonorogenic alkalic rocks, South Eastern Desert, Egypt. In: Proc 5th conf Afr geol
- Helba HA (1994) Geochemical prospecting for rare metals in Nuweibi area, central Eastern desert, Egypt. PhD thesis, Alexandria University, pp 145
- Helba RB, Trumbull G, Morteani SO, Khalil A, Arslan AI (1997) Geochemical and petrographic studies of Ta mineralization in the Nuweibi albite granite complex, Eastern Desert, Egypt. *Miner Depos* 32:164–179. doi: [10.1007/s001260050082](https://doi.org/10.1007/s001260050082)
- Holtz F, Pichavant M, Barbey P, Johannes W (1992) Effect H_2O on liquidus phase relations in the haplogranite system at 2 and 5 kbar. *Am Miner* 77:1233–1244
- Höy T, Kwong YJT (1986) The Mount Grace carbonatite—a Nb and light rare earth element-enriched marble of probable pyroclastics origin in the Shuswap complex, Southeastern British Columbia. *Econ Geol* 81:1374–1386
- Iizumi S, Maehara K, Morris PA, Sawada Y (1994) Sr isotope data of some GSJ rock reference samples. *Mem Fac Sci Shimane Univ* 28:83–86
- Iizumi S, Morris PA, Sawada Y (1995) Nd isotope data for GSJ reference samples JB-1a, JB-3 and JG-1a and the La Jolla standard. *Mem Fac Sci Shimane Univ* 29:73–76
- Jarrar GH, Manton WI, Stern RJ, Zachmann D (2008) Late Neoproterozoic A-type granites in the northernmost Arabian–Nubian Shield formed by fractionation of basaltic melts. *Chem Erde Geochem* 68:295–312. doi: [10.1016/j.chemer.2006.09.002](https://doi.org/10.1016/j.chemer.2006.09.002)
- Katzir Y, Eyal M, Litvinovsky BA, Jahn BM, Zanilevich AN, Valley JW, Beeri Y, Shimshilashvili E (2007) Petrogenesis of A-type granites and origin of vertical zoning in the Katharina pluton, Gebel Mussa (Mt Moses) area, Sinai, Egypt. *Lithos* 95:208–228. doi: [10.1016/j.lithos.2006.07.013](https://doi.org/10.1016/j.lithos.2006.07.013)
- Kimura JI, Yamada Y (1996) Evaluation of major and trace element XRF analyses using a flux to sample ratio of two to one glass beads. *J Miner Petrol Econ Geol* 91:62–72. doi: [10.2465/ganko.91.62](https://doi.org/10.2465/ganko.91.62)
- Kimura JI, Yoshida T, Takaku Y (1995) Igneous rock analysis using ICP-MS with internal standardization, isobaric ion overlap correction, and standard addition methods. *Sci Rep Fukushima Univ* 56:1–12
- Kimura JI, Manton WI, Sun CH, Iizumi S, Yoshida T, Stern RJ (2002) Chemical diversity of the Ueno Basalts, central Japan: identification of mantle and crustal contributions to arc basalts. *J Petrol* 43:1923–1946. doi: [10.1093/petrology/43.10.1923](https://doi.org/10.1093/petrology/43.10.1923)
- Kinnaird JA, Bowden P (1991) Magmatism and mineralization associated with Phanerozoic Anorogenic Plutonic complexes of the African plate. In: Kampunzu A, Lubala RT (eds) The phanerozoic African plate. Springer, Berlin, pp 410–485
- Kovalenko VI (1978) The genesis of rare metal granitoids and related ore deposits. In: Stempok M, Burnol L, Tischendorf G (eds) Metallization associated with acid magmatism Czech geological survey, 3, pp 235–247
- Kröner A (1985) Ophiolites and the evolution of tectonic boundaries in the late Proterozoic Arabian–Nubian Shield of northeast Africa and Arabia. *Precam Res* 27:277–300. doi: [10.1016/0301-9268\(85\)90016-6](https://doi.org/10.1016/0301-9268(85)90016-6)
- Kröner A, Greiling R, Reischmann T, Hussein IM, Stern RJ, Durr S, Kruger J, Zimmer M (1987) Pan-African crustal evolution in northeast Africa. In: Kröner A (ed) Proterozoic lithospheric evolution, geodynamic series 17. American Geophysical Union, pp 235–257
- Le Bas MJ (1981) Carbonatite magmas. *Miner Mag* 44:56–65. doi: [10.1180/minmag.1981.044.334.02](https://doi.org/10.1180/minmag.1981.044.334.02)
- Le Bas MJ, Subbarao KV, Walsh JN (2002) Metacarbonatite or marble? The case of the carbonate, pyroxenite, calcite-apatite rock complex at Borra, Eastern Ghats, India. *J Asian Earth Sci* 20:127–140. doi: [10.1016/S1367-9120\(01\)00030-X](https://doi.org/10.1016/S1367-9120(01)00030-X)
- Le Maitre RW (ed) (2002) Igneous rocks: a classification and glossary of terms. Cambridge University Press, Cambridge
- Lentz DR (1999) Carbonatite genesis: a reexamination of the role of intrusion-related pneumatolytic skarn processes in limestone melts. *Geology* 27:335–338. doi: [10.1130/0091-7613\(1999\)027<0335:CGAROT>2.3.CO;2](https://doi.org/10.1130/0091-7613(1999)027<0335:CGAROT>2.3.CO;2)
- Liu Y, Berner Z, Massonne H, Zhong D (2006) Carbonatite-like dykes from the eastern Himalayan syntaxis: geochemical, isotopic, and petrogenetic evidence for melting of metasedimentary carbonate rocks within the orogenic crust. *J Asian Earth Sci* 26:105–120. doi: [10.1016/j.jseaes.2004.10.003](https://doi.org/10.1016/j.jseaes.2004.10.003)
- Loizenbauer J, Wallbreeher E, Fritz H, Neumayr P, Khudeir AA, Kloetzli U (2001) Structural geology, simple zircon ages and fluid inclusion studies of the Meatiq metamorphic core complex: implications for Neoproterozoic tectonics in the Eastern Desert of Egypt. *Precam Res* 110:357–383. doi: [10.1016/S0301-9268\(01\)00176-0](https://doi.org/10.1016/S0301-9268(01)00176-0)
- Lowell JD, Guilbert JM (1970) Lateral and vertical alteration-mineralization zoning in porphyry ore deposits. *Econ Geol* 65:373–408
- Lowenstern JR, Clynne NA, Bullen TD (1997) Comagmatic A-type granophyre and rhyolites from the Alid Volcanic Center, Eritrea Northeast Africa. *J Petrol* 38:1707–1721. doi: [10.1093/petrology/38.12.1707](https://doi.org/10.1093/petrology/38.12.1707)
- Ludwig KR (2001) Isoplot/Ex, rev. 2.49. A geochronological toolkit for microsoft excel. Berkeley Geochronology Center, Special Publication No. 1a
- Macdonald R, Kjarsgaard BA, Skilling IP, Davies GR, Hamilton DL, Black S (1993) Liquid immiscibility between trachyte and carbonate in ash flow tuffs from Kenya. *Contrib Miner Petrol* 114:276–287. doi: [10.1007/BF00307762](https://doi.org/10.1007/BF00307762)
- Madbouly MI (1991) Petrology and geochemistry of some mafic ultramafic rocks of Sinai, Egypt. MSc thesis, Cairo University, pp 132
- Martin RF, Bonin B (1976) Water and magma genesis: the association hypersolvus granite-subsolvus granite. *Can Miner* 14:228–237
- McKay GA (1989) Partitioning of rare earth elements between major silicate minerals and basaltic melts. In: Lipin BR, McKay GA (eds) Geochemistry and mineralogy of rare earth elements. *Miner Soc Amer* 21: 45–77
- Moghazi AM (1994) Geochemical and radiogenic isotope studies of some basement rocks at the Kid area, Southeastern Sinai, Egypt. PhD thesis, Alexandria University, Egypt

- Moghazi AM, Andersen T, Oweiss GA, Bouseily AM (1998) Geochemical and Sr–Nd–Pb isotopic data bearing on the origin of Pan-African granitoids in the Kid area, Southeast Sinai, Egypt. *J Geol Soc Lond* 155:697–710. doi:10.1144/gsjgs.155.4.0697
- Moussa HE (2002) Mineral chemistry and geochemistry of some mafic-ultramafic intrusions in the South Eastern Desert and Sinai, Egypt. *Egypt J Geol* 46:213–238
- Moussa EMM, Stern RJ, Manton WI, Ali KA (2008) SHRIMP zircon dating and Sm/Nd isotopic investigations of Neoproterozoic granitoids, Eastern desert, Egypt. *Precam Res* 160:341–356. doi:10.1016/j.precamres.2007.08.006
- Mushkin A, Navon O, Halicz L, Hartmann G, Stein M (2003) The petrogenesis of A-type magmas from the Amram Massif, Southern Israel. *J Petrol* 44:815–832. doi:10.1093/petrology/44.5.815
- Nesbitt HW, Young GM (1982) Early Proterozoic climates and plate motions inferred from major element chemistry of lutites. *Nature* 299:715–717. doi:10.1038/299715a0
- Palache C, Berman H, Frondel C (1951) The system of mineralogy of James Dwight Dana and Edward Salisbury Dana, Yale University 1837–1892, vol II: halides, nitrates, borates, carbonates, sulfates, phosphates, arsenates, tungstates, molybdates, etc., 7th edn. Wiley, New York, p 162 (revised and enlarged)
- Pearce JA, Parkinson IJ (1993) Trace element models for mantle melting: application to volcanic arc petrogenesis. In: Prichard HM, Alabaster T, Harris NBW, Neary CR (eds) *Magmatic processes and plate tectonics*, vol 76. *Geol Soc Spec Pub*, pp 373–403
- Pell J, Höy T (1989) Carbonatites in a continental margin environment—the Canadian Cordillera. In: Bell K (ed) *Carbonate—genesis and evolution*. Unwin Hyman, London, pp 200–220
- Reymer APS (1983) Metamorphism and tectonics of Pan-African terrain in Southeastern Sinai. *Precam Res* 19:225–238. doi:10.1016/0301-9268(83)90015-3
- Riad AM (1979) Geology and petrology on some apogranite occurrence, Nuweibi area, Eastern Desert, Egypt. M.Sc. thesis, Al-Azhar University of Cairo, pp 132
- Rollinson H (1994) *Using geochemical data: evaluation, presentation, interpretation*. Longman/Wiley, London/New York, p 352
- Rugless CS, Pirajno F (1996) Geology and geochemistry of the Copperhead albitite “carbonate” complex, east Kimberley, Western Australia. *Aust Earth Sci* 43:311–322. doi:10.1080/08120099608728258
- Sabet AH, Tsogoev VB, Baburin LM, Raid AM, Zakhari A, Armanius LK (1976a) Geologic structure and laws of localization of tantalum mineral zonation at the Nuweibi deposit. *Ann Geol Surv Egypt* VI:119–156
- Sabet AH, Tsogoev VB, Baburin LM, Zharkov VM (1976b) Manifestation of rare metal mineralization of apogranite type in the central Eastern desert of Egypt. *Ann Geol Surv Egypt* VI:75–95
- Samoilov VS (1991) The main geochemical features of carbonatites. *J Geochem Explor* 40:251–262. doi:10.1016/0375-6742(91)90041-R
- Santosh M, Omori S (2008) CO₂ windows from mantle to atmosphere: models on ultrahigh-temperature metamorphism and speculations on the link with melting of snowball Earth. *Gond Res* 14:82–96. doi:10.1016/j.gr.2007.11.001
- Schwartz MO (1992) Geochemical criteria for distinguishing magmatic and metasomatic albite-enrichment in granitoids: examples from the Ta–Li granite Yichun (China) and the Sn–W deposit Tikus (Indonesia). *Miner Depos* 27:101–108. doi:10.1007/BF00197092
- Scogings AJ, Forster IF (1989) Gneissose carbonatites in the Bull, s Run complex, Natal. *S Afr Geol* 92:1–10
- Serencsits CM, Faul H, Foland KA, El-Ramly MF, Hussein AA (1979) Alkaline ring complexes in Egypt: their ages and relationship to tectonic development of the Red Sea. *Ann Geol Surv Egypt* 9:102–116
- Shahien MG (2002) *Petrochemistry and petrogenesis of Kid granitoids, South Eastern Sinai, Egypt*. 6th Inter Conf Geol Arab Word, Cairo University, pp 101–118
- Shimron AE (1975) Petrogenesis of the Tarr albitite–carbonatite complex, Sinai Peninsula. *Miner Mag* 40:13–24. doi:10.1180/minmag.1975.040.309.03
- Shimron AE (1980) Proterozoic island arc volcanism and sedimentation in Sinai. *Precam Res* 12:437–458. doi:10.1016/0301-9268(80)90039-X
- Shimron AE, Brookins DG, Magaritz M, Bartov Y (1973) Origin of the intrusive carbonate rocks between the Gulf of Elat and Gulf of Suez Rifts. *Isr J Earth Sci* 22:243–254
- Soliman KA, Tolba ME, El-Manakhly MM, Madbouly ME, Hasan MM, Abd El Magid EA, Khyamy AA, Abd El Mola AF, Mohamed HA (1992) Geology of the albitite rock, Wadi El-Tarr, Southern Sinai. *Ann Geol Surv Egypt* 18:29–37
- Srivastava RK, Heaman LM, Sinha AK, Shiha S (2005a) Emplacement age and isotope geochemistry of Sung Valley alkaline-carbonatite complex, Shillong Plateau, northeastern India: implications for primary carbonate melt and genesis of the associated silicate rocks. *Lithos* 81:33–54. doi:10.1016/j.lithos.2004.09.017
- Srivastava RK, Mohan A, Filho CFF (2005b) Hot-fluid Driven Metasomatism of Samalpatti carbonatites, South India: evidence from petrology, mineral chemistry, trace elements and stable isotope compositions. *Gond Res* 8:77–85. doi:10.1016/S1342-937X(05)70264-1
- Stacey JS, Kramers JD (1975) Approximation of terrestrial lead isotope evolution by a 2-stage model. *Earth Planet Sci Lett* 26:207–221
- Steiger RH, Jäger E (1977) Subcommittee on geochronology: convention of the use of decay constants in geo- and cosmochronology. *Earth Planet Sci Lett* 36:359–362
- Stern RJ (1981) Petrogenesis and tectonic setting of late Precambrian ensimatic volcanic rocks, central Eastern desert of Egypt. *Precam Res* 16:195–230. doi:10.1016/0301-9268(81)90013-9
- Stern RJ (1985) The Najd Fault System, Saudi Arabia and Egypt: a late Precambrian rift-related transform system. *Tectonics* 4:497–511. doi:10.1029/TC004i005p00497
- Stern RJ (1994) Arc assembly and continental collision in the Neoproterozoic East African Orogen: implications for the consolidation of Gondwanaland. *Annu Rev Earth Planet Sci* 22:319–351
- Stern RJ (2002) Crustal evolution in the East African Orogen: a Neodymium isotopic perspective. *J Afr Earth Sc* 34:109–117. doi:10.1016/S0899-5362(02)00012-X
- Stern RJ, Gwinn CJ (1990) Origin of late Precambrian intrusive carbonates, Eastern Desert of Egypt and Sudan: C, O and Sr isotopic evidence. *Precam Res* 46:259–272. doi:10.1016/0301-9268(90)90005-B
- Stern RJ, Gottfried D, Hedge CE (1984) Late Precambrian rifting and crustal evolution in the Northeastern Desert of Egypt. *Geology* 12:168–171. doi:10.1130/0091-7613(1984)12<168:LPRACE>2.0.CO;2
- Streckeisen A (1980) Classification and nomenclature of volcanic rocks, lamprophyres, carbonatites and melilitic rocks IUGS Subcommittee on the systematics of igneous rocks. *Geol Rundsch* 69:194–207. doi:10.1007/BF01869032
- Taubald H, Morteani G, Satir M (2004) Geochemical and isotopic (Sr, C, O) data from the alkaline complex of Grønødal-I’ka (South Greenland): evidence for unmixing and crustal contamination. *Int J Earth Sci* 93:348–360. doi:10.1007/s00531-004-0392-9
- Tuttle CF, Bowen NL (1958) Origin of granite in the light of experimental studies in the system NaAlSi₃O₈–KAlSi₃O₈–SiO₂–H₂O. *Geol Soc Am Memoir* 74:153

- Wagner C, Mokhtari A, Deloule E, Chabreaux F (2003) Carbonatite and alkaline magmatism in Taourirt (Morocco): petrological, geochemical and Sr–Nd isotope characteristics. *J Petrol* 44:937–965. doi:10.1093/petrology/44.5.937
- Whitehouse MJ, Kamber BS (2005) Assigning dates to thin gneissic veins in high-grade metamorphic terranes: a cautionary tale from Akilia, southwest Greenland. *J Petrol* 46:291–318
- Whitehouse MJ, Kamber B, Moorbath S (1999) Age significance of U–Th–Pb zircon data from early Archaean rocks of west Greenland—a reassessment based on combined ion-microprobe and imaging studies. *Chem Geol* 160:201–224
- Wiedenbeck M, Allé P, Corfu F, Griffin WL, Meier M, Oberli F, von Quadt A, Roddick JC, Spiegel W (1995) Three natural zircon standards for U–Th–Pb, Lu–Hf, trace element and REE analysis. *Geostandards News* 19:1–23
- Woolley AR (2003) Igneous silicate rocks associated with carbonatites: their diversity, relative abundance and implications for carbonatite genesis. *Period Miner* 72:9–17
- Woolley AR, Kempe PRC (1989) Carbonatites: nomenclature, average chemical composition and element distribution. In: Bell K (ed) *Carbonatites: genesis and evolution*. Unwin Hyman, London, pp 1–14
- Wyllie PJ, Tuttle OF (1960) The system CaO–CO₂–H₂O and the origin of carbonatites. *J Petrol* 1:1–46